Mass Spectrometry-based Profiling of Single-cell Histone Post-translational Modifications to Dissect Chromatin Heterogeneity

Ronald Cutler[1,2,=,*] Laura Corveleyn[3,=], Claudia Ctortecka[4,=], Joshua Cantlon[5], Sebastian Alvaro Jacome Vaca[6], Dieter Deforce[3], Jan Vijg[1,7], Maarten Dhaenens[3], Malvina Papanastasiou[4], Steven A. Carr[4], and Simone Sidoli[2,*]

[1] Department of Genetics, Albert Einstein College of Medicine, Bronx, NY, USA.

[2] Department of Biochemistry, Albert Einstein College of Medicine, Bronx, NY, USA.

[3] ProGenTomics, Laboratory of Pharmaceutical Biotechnology, Department of Pharmaceutics, Ghent University, Ghent, Belgium.

[4] Broad Institute of MIT and Harvard, Cambridge, MA, USA.

[5] SCIENION US Inc., Phoenix, AZ, USA.

[6] BioNTech, Cambridge, MA, USA

[7] Center for Single-Cell Omics, School of Public Health, Shanghai Jiao Tong University School of Medicine, Shanghai 200025, China

[=] Authors contributed equally to this work

[*]Correspondence to R.C. (ronald.cutler@einsteinmed.edu) and S.S. (simone.sidoli@einsteinmed.edu)

Abstract

The emerging popularity of single-cell sequencing technologies has revealed unexpected heterogeneity of chromatin states and gene expression in seemingly homogeneous cell populations. Similarly, single-cell proteomics has proven capable of quantifying heterogeneity of proteomes amongst single cells, yet, due to their low stoichiometry, it remains limited in investigating the heterogeneity of protein post-translational modifications (PTMs). Here, we present a robust mass spectrometry-based method for the unbiased analysis of histone PTMs (hPTMs) at single-cell level, in order to investigate the complex relationship between the regulation of epigenetic marks and cell identity. Our method identified both single and combinatorial hPTMs (68 peptidoforms in total), including nearly all of the most studied hPTMs. We demonstrate technical reproducibility comparable to traditional ‘bulk’ experiments. Furthermore, our platform distinguishes/removes technical noise from true biological cell-to-cell variation of hPTM abundances. As a proof of concept, we treated cells with sodium butyrate, a histone deacetylase inhibitor, and demonstrated that our method can i) distinguish between treated and non-treated cells, ii) identify sub-populations of cells that respond differently to treatment, and iii) reveal differential co-regulation of hPTMs in the context of drug treatment. Overall, these experiments establish the applicability of our method to investigate chromatin heterogeneity at the single-cell resolution, which has important implications for understanding complex conditions like cancer and aging. In addition, this method provides new opportunities for analyzing the 'histone code' by utilizing cellular heterogeneity in covariation analysis.

Keywords: single-cell, proteomics, histones, post-translational modifications, chromatin, mass spectrometry, heterogeneity, covariance, histone deacetylase inhibitor

Introduction

Epigenetic states are imprinted through chemical modifications to DNA and associated histone proteins that describe the complex relationship between the epigenome and cellular phenotypes[1]. The 'histone-code' describes the complex interplay between diverse post-translational modifications (PTMs) of histones[2]. The most prevalent hPTMs (hPTMs) encompass acetylation (ac), methylation (me), ubiquitination (ub), and phosphorylation (ph). These hPTMs contribute to the modulation of chromatin structure through their distinct chemical properties and their capacity to attract chromatin-modifying enzymes and binding proteins, thereby influencing gene expression. For instance, histone 4 lysine 16 acetylation (H4K16ac) decompacts chromatin structure and thereby increases gene transcription[3]. In contrast, trimethylation of histone 3 lysine 27 (H3K27me3) is generally associated with transcriptional repression and has been implicated in epigenetic reprogramming[4,5]. Notably, several hPTMs have been linked to multiple diseases, including various forms of cancer, neurodegenerative and autoimmune diseases [6–9]. For example, loss of H4K16ac and H4K20me3 are common hallmarks of cancer.

Bulk analysis of hPTMs, in which histones are extracted from cells at high purity[10], has markedly improved our understanding of their pivotal role in health and disease. However, these bulk methods often require substantial input material (typically 1 million cells), which limits their use in cases when the sample input is low (e.g. clinical specimens) [11,12]. Additionally, established single-cell sequencing methods, such as single-cell RNA-sequencing, have showcased that conventional analyses of large cell populations mask the inherent cell-to-cell variability, therefore limiting the ability to uncover subtle differences that may drive disease progression[13]. Single-cell analysis enables the identification of rare cell subpopulations, thereby offering insights into cellular heterogeneity, transitions, and responses to stimuli, which has shown significant relevance in cancer and aging research[14–17]. For example, in the context of cancer, single-cell resolution is essential for precisely identifying therapy-resistant subpopulations that may emerge and lead to minimal residual disease[18]. Additionally, cancer stem cells are often small heterogeneous populations of a few thousand cells that express significantly different populations of RNAs and proteins[19].

Over the past decade, several methods have been introduced to analyze hPTMs from single cells, mostly by miniaturizing bulk sequencing methods, such as single-cell chromatin immunoprecipitation sequencing (scChiPseq)[13,20–22]. Despite successfully identifying hPTMs in single cells at specific genomic loci, the limited throughput and labor-intensive nature of these protocols hinder their extensive application in a broader setting. More recently, Cheung et al.

developed EpiTOF, for simultaneous profiling of 60 epigenetic targets in a single-cell using heavy metal isotope-labeled antibodies and mass cytometry by time-of-flight[5]. Applying their method to profile human immune cells, the authors distinguished cell type-specific hPTMs patterns and demonstrated increasing cell-to-cell variability with age, providing valuable insight into the role stochastic changes play in the complex process of aging which is still poorly understood. However, all these approaches rely on antibodies, which suffer from i) cross-reactivity, ii) steric hindrance when targeting combinatorial hPTMs, iii) limited number of targets, iv) quantitative ambiguity resulting from differences in affinity, v) lack of multiplexing, and vi) limited detection of novel modifications[23,24].

In contrast, liquid chromatography coupled with tandem mass spectrometry (LC-MS/MS) provides a comprehensive view of the epigenetic landscape through the direct and quantitative measurement of multiple histone modifications[25,26]. Recent advances in MS instrumentation have improved sensitivity, quantitative accuracy, and throughput, making MS the gold standard for global single-cell proteomics[27,28]. Although histones are commonly identified in such workflows due to their abundance within the cell, a comprehensive method for studying hPTMs at the single-cell level is currently lacking.

Here, we present a method that reliably quantifies hPTMs on canonical histones H1, H2A, H2B, H3 and H4 from single mammalian cells using label-free LC-MS/MS that we call schPTM (single-cell histone post-translational modifications). We combine single-cell dispensing and semi-automated sample preparation using the cellenONE with data independent acquisition (DIA) on the timsTOF Ultra (Bruker). Our workflow allows for the accurate quantification of 68 histone peptidoforms in a single run, comprising a total of 25 unique PTMs. We demonstrate the sensitivity and quantitative accuracy of our workflow by comparing our schPTM abundances to background noise, titration curves, and bulk samples. In addition, we perform a thorough analysis of the technical noise inherent to ultra-low input methods allowing us to identify cell-to-cell biological noise. As a proof of concept, we treat single cells with a histone deacetylase (HDAC) inhibitor and show that our method can differentiate between control and treated cells and capture heterogeneity in treatment response. Analysis of PTM-PTM correlations at the single-cell level reveals crosstalk (co-regulation) between histone modifications in cells in homeostasis, which is significantly disrupted by HDAC inhibitor treatment.

Results

Identification of hPTMs at single-cell resolution using LC-MS/MS

In bulk histone analysis, histones are typically extracted from cells using acid extraction followed by trichloroacetic acid (TCA) precipitation[10,29]. Histones are subsequently propionylated with propionic anhydride at the protein and peptide level to modify N-termini and free lysines and increase the size and hydrophobicity of the peptides prior to LC-MS/MS analysis. Manual execution of the multistep protocol is widely employed, though fully automated protocols using liquid handling automation have been developed enabling the large profiling of hPTMs upon chemical perturbations in multiple biological backgrounds[30].

We introduce a protocol for semi-automated histone sample preparation of single mammalian cells using the cellenONE picoliter dispensing platform (Cellenion), which is commonly employed in global single-cell proteomics (SCP) workflows[28,31,32]. Its controlled environment and high dispensing accuracy reduce technical variability and adsorptive losses that result from manual sample preparation steps, which are significant when working with single cells.

We directly isolate single cells to a 384-well plate (**Supplementary Figs. 1A-D)** pre-filled with 1 µL lysis buffer, consisting of 0.2% (w/v) n-Dodecyl β-D-maltoside (DDM) in 1M Triethylammonium bicarbonate (TEAB)[33]. The 384-well plate was sealed with adhesive aluminum foil, vortexed for 5 sec, and centrifuged at 500 g for 30 sec. To overcome elevated evaporation and possible incomplete sealing of the plate, the outermost wells were excluded from sample processing. Histones were derivatized by dispensing 100 nl propionic anhydride and incubation for 30 min at room temperature (**Supplementary Figs. 1E-G)**. The plate was dried on the heated plate holder at 50°C within the cellenONE to ensure evaporation of propionylation reagents and reduce background signal noise. Histones were digested using trypsin (3 ng per sample) by dispension of 1 µl mastermix and incubated for 2 hrs at 50°C within the cellenONE. Peptides underwent a secondary derivatization step as described above to modify the newly formed N-termini and improve chromatographic retention. Following reagent addition to the wells, the plate was resealed with aluminum foil, vortexed and centrifuged at 500 g for 30 sec to ensure sufficient mixing. We verified the efficiency of derivatization, as a low percentage of propionylation would lead to small and hydrophilic peptides that are difficult to detect by MS and therefore result in a lower signal-to-noise ratio. To do this, we looked for tryptic and ArgC specific peptides with variable propionylation on lysines and N-termini using data-dependent and data-independent acquisition methods. Overall, over 75% of unique peptides are propionylated in single cells (**Supplementary Figs. 2A-D)**.

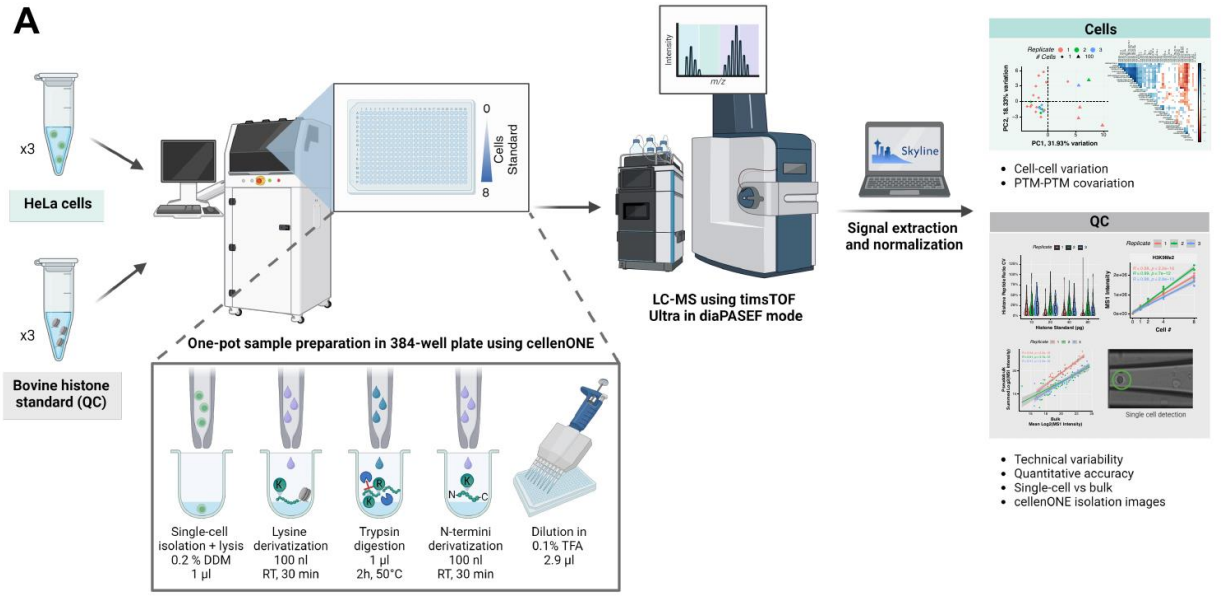
A
x3
HeLa cells
x3
Bovine histone standard (QC)
0
Cells
Standard
8
One-pot sample preparation in 384-well plate using cellenONE
Single-cell isolation + lysis 0.2 % DDM 1 µl
Lysine derivatization 100 nl RT, 30 min
Trypsin digestion 1 µl 2h, 50°C
N-termini derivatization 100 nl RT, 30 min
Dilution in 0.1% TFA 2.9 µl
LC-MS using timsTOF Ultra in diaPASEF mode
Skyline
Signal extraction and normalization
Cells
Cell-cell variation
PTM-PTM covariation
QC
Technical variability
Quantitative accuracy
Single-cell vs bulk
cellenONE isolation images

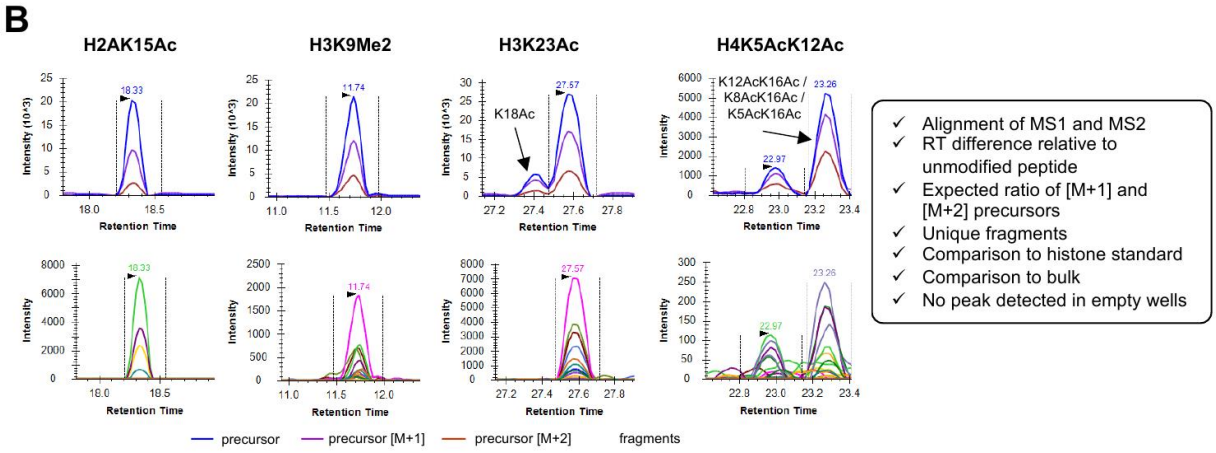
B
H2AK15Ac
H3K9Me2
H3K23Ac
H4K5AcK12Ac
K18Ac
K12AcK16Ac / K8AcK16Ac / K5AcK16Ac
Retention Time
Intensity
precursor
precursor [M+1]
precursor [M+2]
fragments
Alignment of MS1 and MS2
RT difference relative to unmodified peptide
Expected ratio of [M+1] and [M+2] precursors
Unique fragments
Comparison to histone standard
Comparison to bulk
No peak detected in empty wells

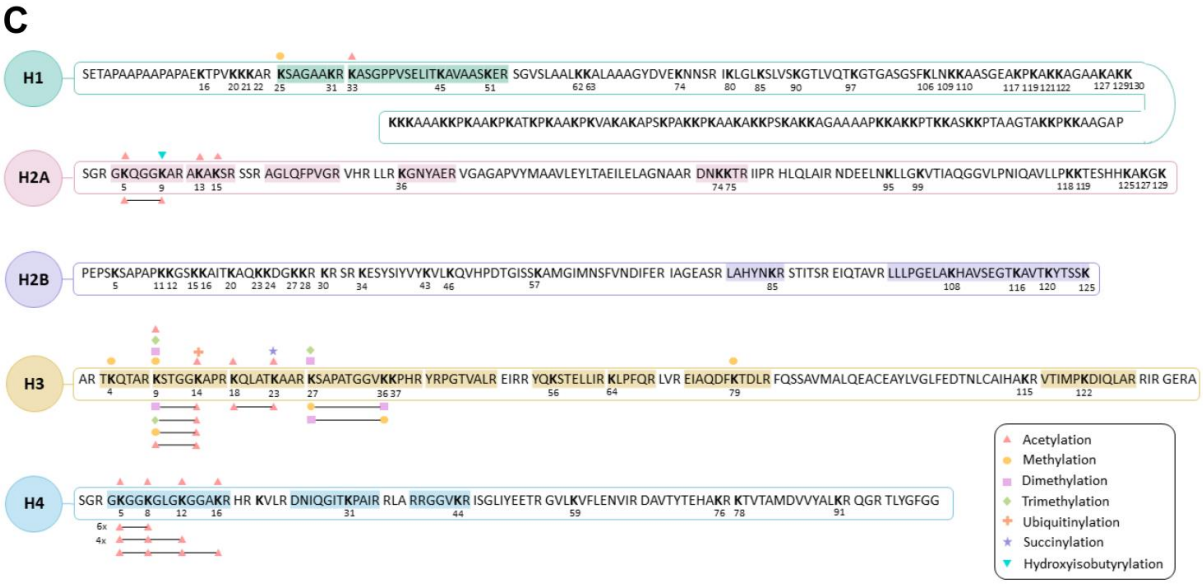
C
H1
SETAPAAPAAPAPAEKTPVKKKAR KSAGAAKR KASGPPVSELITKAVAASKER SGVSLAALKKALAAAGYDVEKNNSR IKLGLKSLVSKGTLVQTKGTGASGSFKLNKKAASGEAKPKAKKAGAAKAKK
KKKAAAKKPKAAKPKATKPKAAKPKVAKAKAPSKPAKKPKAAKAKKPSKAKKAGAAAAPKKAKKPTKKASKKPTAAGTAKKPKKAAGAP
H2A
SGR GKQGGKAR AKAKSR SSR AGLQFPVGR VHR LLR KGNYAER VGAGAPVYMAAVLEYLTAEILELAGNAAR DNKKTR IIPR HLQLAIR NDEELNKLLGKVTIAQGGVLPNIQAVLLPKKTESHHKAKGK
H2B
PEPSKSAPAPKKGSKKAITKAQKKDGKKR KR SR KESYSIYVYKVLKQVHPDTGISSKAMGIMNSFVNDIFER IAGEASR LAHYNKR STITSR EIQTAVR LLLPGELAKHAVSEGTKAVTKYTSSK
H3
AR TKQTAR KSTGGKAPR KQLATKAAR KSAPATGGVKKPHR YRPGTVALR EIRR YQKSTELLIR KLPFQR LVR EIAQDFKTDLR FQSSAVMALQEACEAYLVGLFEDTNLCAIHAKR VTIMPKDIQLAR RIR GERA
H4
SGR GKGGKGLGKGGAKR HR KVLR DNIQGITKPAIR RLA RRGGVKR ISGLIYEETR GVLKVFLENVIR DAVTYTEHAKR KTVTAMDVVYALKR QGR TLYGFGG
Acetylation
Methylation
Dimethylation
Trimethylation
Ubiquitinylation
Succinylation
Hydroxyisobutyrylation

Fig. 1 | Overview of schPTM method and 68 identified peptidoforms. A) Schematic overview of the method, from left-to-right: 1) Suspensions of single cells or histone standards were isolated and prepared within the wells of a 384-well plate using the liquid handling capabilities of the cellenONE instrument, 2) Histone peptidoforms were acquired using the Vanquish LC and TimsTof Ultra MS instruments, 3) Data analysis was performed with Skyline and custom R scripts. For details on cellenONE cell isolation and preparation see (**Supplementary Fig. 1**). **B)** Extracted ion chromatograms (XICs) of MS1 precursor (top panels) and MS2 fragments (bottom panels) for four representative histone peptidoforms in a representative single-cell. Peaks are picked based on criteria shown in box on right side. For additional XICs of isobaric peptides see (**Supplementary Fig. 3A**). **C)** Overview of the histone peptidoforms identified by our method. Peptide sequences highlighted were detected by our method. PTMs are represented by symbols shown in the legend on right side. Single PTMs are shown on top of sequences, while combinatorial PTMs are shown by a connecting line underneath the sequence. For proportions of each modification see (**Extended Data Fig. 1A**).

Finally, samples were diluted manually and stored at -80 °C until LC-MS/MS analysis. Our method adds to current SCP workflows by demonstrating the feasibility of chemical derivatization of peptides by dispensing ultra-low amounts (100 nl) of the low-viscosity derivatization reagent during preparation with the celleONE instrument. Because of the volatile nature of derivatization reagent, this dispensing method required fine-tuning of the piezo dispensing capillary nozzle parameters to obtain a stable droplet (**Supplementary Fig. 1E; Methods**).

For technical quality control, we prepared bulk samples consisting of 1 µL of ~100 cells in the lysis buffer which were processed identically to the single cells. For calculating quantitative accuracy, we dispensed a titration curve of either varying amount of cells as well as pure bovine histones representing 1, 2, 4 and 8 cells (corresponding to 10, 20, 40 and 80 pg of bovine histone, respectively). The cellenONE automatically records images of the glass nozzle prior to cell dispensing, which we use to control for contaminating particles within the ejection volume and verify the dispense of a single-cell (**Supplementary Figs. 1A-D**). Moreover, top views of all wells in the 384-well plate pre- and post-buffer addition were recorded to monitor successful dispensing (**Supplementary Figs. 1F-G**). The complete experimental workflow is depicted in **Fig. 1A**. To the best of our knowledge, this method represents the first MS-based approach to quantify hPTMs at single-cell resolution in an unbiased manner.

We performed data processing in Skyline using a spectral library derived from bulk samples, with manual adjustment of peak boundaries based on predetermined requirements (**Fig. 1B**, **right box**). For every peptide, MS1 and MS2 signals were aligned, the expected ratio of [M+1] and [M+2] precursor signals were evaluated, the relative difference in retention time was compared to the unmodified form of the peptide and the presence of unique fragments, indicative for a particular PTM, was verified.

For the H4 N-terminal peptide H4 (4-17), encompassing four modifiable lysines, several isobaric forms were detected in different degrees of acetylation that are often co-eluting. Therefore, a combination of unique fragments were used for identification of these peptidoforms (**Supplementary Fig. 3A-B; Methods**). Specifically, we utilized their fragment ion relative ratio to split the intensity of their precursor signal for the different isobaric species.

Following all these criteria, we successfully identified peptides from H1, H2A, H2B, H3, and H4, as well as their variants H1.2, H1.5, H2AJ, H2AX, and H3.3 (**Supplementary Table 1**). PTMs identified included acetylation (Ac), methylation (Me), dimethylation (Me2), trimethylation (Me3), ubiquitinylation (Ub), succinylation (Su) and hydroxyisobutyrylation (Hib) (**Extended Data Fig. 1A**). These were identified either alone (25 peptides) or in combination with other PTMs on a single peptide (43 peptides), resulting in 68 distinct peptidoforms (**Fig. 1C**). Notably, we achieved comprehensive coverage of the N-terminal tails of H3 and H4, in particular of peptides H3(9-17) and H4(4-17) that were identified with multiple peptidoforms, demonstrating the sensitivity of our method. Missing regions included the H2B N-terminus and H1 C-terminus that lack arginine residues, resulting in long and hydrophobic peptides. These peptides are subject to poor HPLC separation, which is additionally challenged by ambiguous identifications due to several peptidoforms sharing the same precursor mass.

Benchmarking of schPTM quantification

To benchmark quantitative aspects of our method, we prepared 3 batches on separate days (**Supplementary Table 2)**, totaling 60 samples of varying amounts of cells (**Extended Data Figs. 1B-C**). We consistently detected 68 histone peptides across all samples with < 0.1% missing values (**Extended Data Fig. 1D**), highlighting the strength of the DIA acquisition method. Due to the expectedly low peptide input derived from a single-cell, to distinguish between signal and measurement noise and benchmark the specificity of the measured peptides at the MS1 level, we compared the raw intensities of single-cell samples to ‘empty wells’, which included all reagents with no cells added. We found that the MS1 signal intensities in the 1 cell samples were on average ~9.5X above the noise level in empty wells (**Fig. 2A** and **Extended Data Figs. 2A-B**).

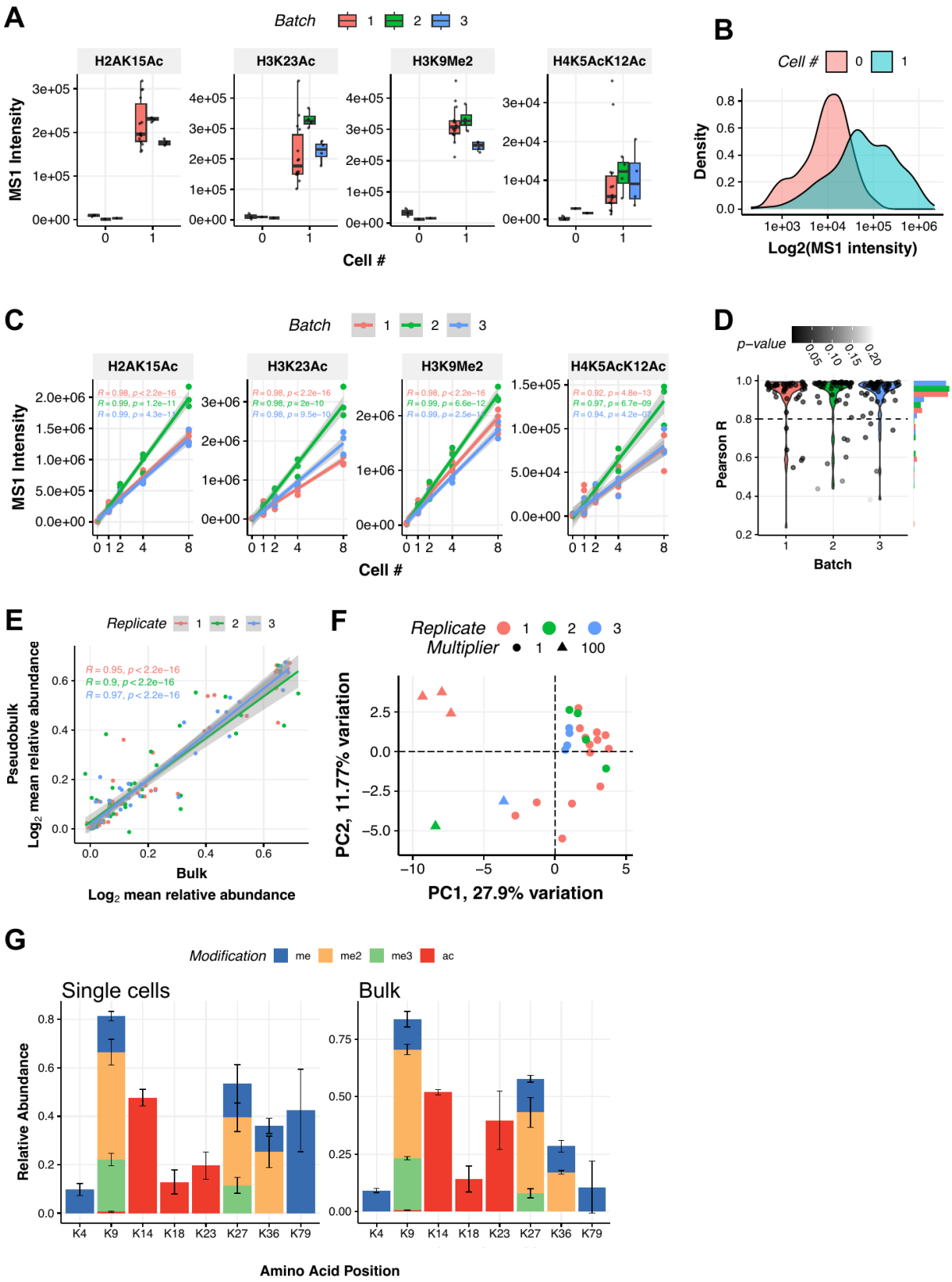

Fig. 2 | schPTM quantification enabled by high sensitivity and precision. A) Comparison of raw MS1 intensity of empty wells (Cell # 0) and wells containing single cells (Cell # 1) for 4 representative histone

peptidoforms for each batch. For all peptidoforms see (**Extended Data Fig. 2A**). **B)** Distribution of raw Log_2 MS1 intensities for all histone peptidoforms in all 3 batches for empty wells and wells containing single cells after filtering out peptides with low signal (**Methods**). For each batch separately see (**Extended Data Figs. 2B-C**). **C)** Titration curves for 4 representative histone peptidoforms of raw MS1 intensity where various amounts of cells were prepared in a single-well and then were assessed for linearity. Pearson R correlation coefficients and significance of correlation for each batch is shown. For all peptides see (**Extended Data Fig. 3B**). **D)** Distribution of Pearson R correlation coefficients for titration curves of all histone peptidoforms in each batch. A dashed line is drawn at R=0.8 to indicate the threshold used for filtering out histone peptidoforms deemed to be non-quantifiable. **E)** Correlation of histone peptidoform Log_2 relative abundance between bulk (~100-cell) and 'pseudobulk' (mean of single cells) samples in each batch. For correlation using raw MS1 intensity see (**Extended Data Fig. 6A**). **F)** Principal component analysis of histone peptidoform relative abundances for single-cell and bulk samples. For no batch-correction see (**Extended Data Fig. 5D-F**). For direct comparison of single-cell and bulk samples see (**Extended Data Fig. 6B-C**). **G)** Individual histone PTMs (single and combinatorial PTMs) relative abundances detected on histone H3 in single cells (left panel) and bulk (right panel) samples from all batches. For comparison to previous bulk studies, see (**Extended Data Fig. 6D-E**).

Peptides detected with similar MS1 signal intensities in single-cell samples and 'empty wells' were deemed indistinguishable from background noise and filtered out from subsequent analysis (**Fig. 2B** and **Extended Data Fig. 2C; Methods**). As MS1 intensities in our measurements were on average over ~3X greater than MS2 intensities and suffered less from distortion at lower signal intensities **(Extended Data Fig. 1E**), we chose to quantify histone peptide abundances at the MS1 level, as typically occurs in MS-based histone analysis using EpiProfile[34]. Exceptions to this were co-eluting isobaric modifications of the H4(4-17) histone peptide in which we used MS2 fragment ion intensities to deconvolute the MS1 intensity (**Supplementary Figs. 3A-B; Methods**).

To benchmark the sensitivity and precision of our method we assessed the linearity of signal intensities using a 5-point cell titration curve of varying amounts of cells (i.e. 0, 1, 2, 4, and 8 cells). As expected, the MS1 intensity was proportional to the number of cells across all peptidoforms yielding excellent R values (**Fig. 2C-D**, **Extended Data Fig. 3A**). Peptides with an average Pearson R of less than 0.8 were deemed unquantifiable and excluded from subsequent analysis (**Extended Data Fig. 3B; Methods**).

To next examine whether the MS response of histone peptides measured in cell lysates was similar to histone peptides isolated from cells (bulk-histone workflow), we employed bovine histone standards isolated from cells at varying amounts (0, 10, 20, 40, and 80 pg; 1 cell contains ~6.5 pg of histone protein[35]). These were dispensed at 1 pg/nL with the cellenONE and processed identically to the isolated cells. Comparing respective titration curves at the MS1 level with those the cells described above, we found that these yielded similar results, demonstrating sufficient

sensitivity and precision for hPTM quantification, and further validating our measurements in single cells **(Extended Data Figs. 4A-D**).

To then validate the abundances of single-cell histone peptidoforms relative to bulk samples, we acquired 5 ~100-cell samples across the 3 batches (**Extended Data Figs. 1B-C**). After quality control filtering, normalization, and batch-correction (**Extended Data Figs. 5A-F; Methods**), we were able to quantitatively analyze 55 peptidoforms. We first evaluated the similarity of our single-cell samples to bulk samples by averaging the peptidoform relative abundances across all single cells within each batch to create a 'pseudobulk' sample. We then correlated the 'pseudobulk' peptidoform relative abundances to the average of the bulk samples within each batch, which resulted in an average R value of 0.94 across the 3 batches (**Fig. 2E**). This indicated good agreement between our ultra-low input single cell measurements to those expected from routine bulk hPTM analysis with a sufficient sample amount. Similar results were also obtained when performing the same analysis with unnormalized data (**Extended Data Fig. 6A**). We then performed principal component analysis (PCA) on the relative abundances of all peptidoforms, which revealed separation of the single-cell and bulk samples along the first principal component (PC), and accounted for 27.9% of the variance in the data (**Fig. 2F**). However, the separation between single-cell and bulk samples was limited to small differences as the average difference was only a 1.28×10^{-3} Log_2 fold change, when directly comparing relative abundances of single cells and bulk samples (**Extended Data Figs. 6B-C**). Furthermore, we observed similar profiles of the relative abundances of individual PTMs on histone H3 between single-cell and bulk samples (**Fig. 2G**), in addition to previous bulk studies utilizing HeLa cells **(Extended Data Figs. 6D-E**). Collectively, our findings demonstrate that there were no notable systemic biases in the abundance of hPTMs upon adaptation of our bulk histone workflow to the profiling of single cells.

Biological cell-to-cell variability of schPTMs

To distinguish between biological and technical variability in single-cell samples, we employed the bovine histone standards described in the previous section (**Extended Data Figs. 7A-B**) and calculated the coefficient of variation (CV) of the relative abundances of 55 peptidoforms for the various amounts of histone standards prepared within a batch (intra-) or across batches (inter-). For the 10 pg histone standard, both intra- and inter-CVs showed levels below 25% on average (**Figs. 3A-B**). For data that was unnormalized and not batch-corrected, intra-CVs were similar to the relative abundance data, while inter-CVs were roughly double (**Extended Data Figs. 7C-D**),

indicating the effect of batch-to-batch variation and highlighting the need for normalization and batch-correction.

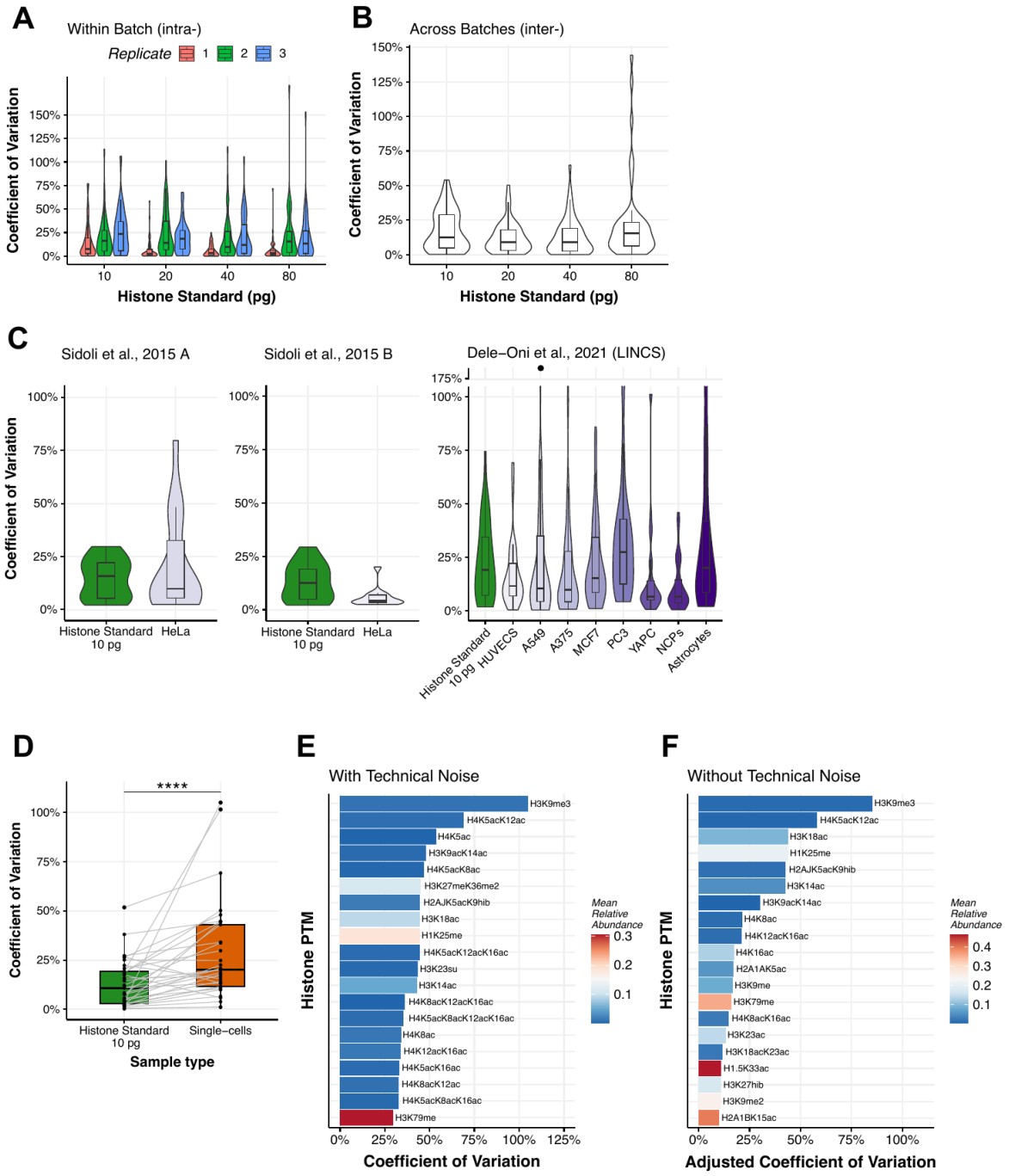

Fig. 3 | Low technical noise allows for analysis of hPTM biological cell-to-cell variability. A-B) Coefficient of variation (CV) of histone peptidoform relative abundances for histone standard technical replicates within each batch (intra-) (**A**) and across the 3 batches (inter-) (**B**). **C)** CV of histone peptidoform relative abundances for 10 pg histone standard technical replicates across all batches compared to bulk technical replicates of HeLa cells (Sidoli et al., 2015 A, 5 replicates, 16 peptidoforms; Sidoli et al., 2015 B,

4 replicates, 12 peptidoforms) and processing replicates of cell lines treated with DMSO in the NIH Library of Integrated Network-Based Cellular Signatures Consortium (Dele-Oni et al., 2021, 3 replicates, 29 peptidoforms). Histone peptidoforms were filtered to match those quantified in each respective study (**Supplementary Table 3**). **D)** CV of histone peptidoform relative abundances for 10 pg histone standard across all batches compared to that of single cells across all batches matched by peptidoform. Statistics: paired Wilcox test, p-value=$1.1*10^{-5}$ (****). **E-F)** CV of histone peptidoform relative abundances of top 20 peptidoforms ranked from highest to lowest amongst single-cells from all 3 batches shown with technical noise (**E**) and without technical noise (i.e. epigenetic noise) (**F**).

To be able to identify subtle biological changes across cells, which may be difficult due to variation across replicates and ultra-low input amounts[36,37], we compared the technical variation of peptidoform levels from the 10 pg standard samples across all batches (roughly equivalent to the amount of histone in a single-cell) to bulk samples from previous studies; these included technical replicates of HeLa cells[30,38,39] and processing replicates of cell lines in the NIH Library of Integrated Network-Based Cellular Signatures consortium[30,38,3940] (**Supplementary Table 3).** We found that the CVs of our 10 pg standard samples are at comparable levels, which highlights the reproducibility of our schPTM workflow and establishes a technical variation baseline for the sample input of a single-cell (**Fig. 3C**).

A critical feature of single-cell analysis is to be able to quantify subtle cell-to-cell biological variation, which can reveal cell states and regulatory relationships inaccessible by bulk analyses.

Our method facilitates this capability because the CVs for peptidoforms across individual cells were significantly higher compared to those observed among technical replicates. (**Fig. 3D**). To then determine biological cell-to-cell variability for individual peptidoforms (i.e. epigenetic noise), we adjusted for the technical noise and ranked peptidoforms from highest to lowest CV (**Fig. 3E; Extended Data Fig. 7E; Methods**)**.** This analysis revealed H3K9me3 and H4K5acK12ac as the most biologically variable peptidoforms in our cell model and H4K12ac, H3K9me3K14ac and H2AJK5acK9ac as the most consistent ones within the analyzed cell population (**Fig. 3F)**.

Distinct schPTM profiles following HDAC inhibitor treatment

To demonstrate the applicability of our approach and detect biologically relevant hPTM abundance changes, we treated HeLa cells with 5 mM of the histone deacetylase (HDAC) inhibitor sodium butyrate (NaBut). NaBut competitively binds to the zinc sites of class I and II HDACs, resulting in hyperacetylation of several histone sites, particularly those located on histones H3 and H4. After a 24-hour incubation, both control (PBS vehicle) and NaBut treated cells were harvested and processed using our schPTM workflow (**Fig. 1A**). Single cells were isolated from

three different cell populations, control, treated, and a 1:1 mixture of control and treated (mixed) (**Fig. 4A; Supplementary Table 4)**. We included a mixed population of cells to evaluate, without prior knowledge of the control or treated groups, if these cells can be blindly classified based on their hPTMs profiles. Similar to previous experiments, we also included 8 ~100-cell bulk samples. Following our quality control and normalization pipeline, we were able to obtain readouts for 53 peptidoforms in 5 control, 12 treated and 33 mixed single cells (**Extended Figs. 8A-E**). Due to the low number of control cells that passed filtering criteria in this experiment, we further included 22 untreated single-cells and 5 ~100-cell bulk samples into the analysis from the benchmarking experiments to increase the number of control cells to a total of 27 and performed batch-correction (**Extended Data Fig. 8F)**. PCA of all 53 peptidoforms revealed clear separation between control and treated cells in PC1, accounting for 27.89% of the variation in the data and was significantly correlated to the NaBut treatment variable ($R=0.66$, $p<0.001$) (**Fig. 4B and Extended Data Figs. 8G-H)**. Mixed cells were uniformly distributed across PC1, as expected. Separation in PC2 was mainly driven by sample amounts (single-cell and 100-cell bulk samples, $R=0.81$, $p<0.001$). (**Fig. 4B and Extended Data Fig. 8H)**.

Next, we classified the cells in the mixed group. As NaBut treatment is known to cause upregulation of hPTM acetylation on histone H4[41], we calculated the relative abundance of the different numbers of acetylations on histone H4 (i.e. mono, di, tri and tetra) and performed PCA with the H4 summarized relative abundances (**Fig. 4C; Methods**). This clearly separated the control and treated cells along PC1 and was significantly correlated to the NaBut treatment variable ($R=0.54$, $p<0.001$) (**Fig. 4C**). However, PC1 now accounted for 70.64% of the variation in the data (compared to 27.89% when using all peptidoforms as shown in **Fig. 4B**). From this, we concluded that H4 acetylation, which is an exclusive modification at the H4 N-terminus (AAs 1-16)[41], can be used to classify the single cells isolated from the mixed population. Thus, after training a k-nearest neighbor (KNN) classifier on the labeled cells, which achieved an accuracy of 84.21%, we classified 16 and 17 of the single cells from the mixed population as control or treated, respectively (**Fig. 4D-E**). This analysis demonstrates the ability of our method to classify cells using global hPTM levels without knowing the assigned condition *a priori*. This type of analysis is applicable when profiling complex populations that contain different cell types or different cellular states at distinct ratios.

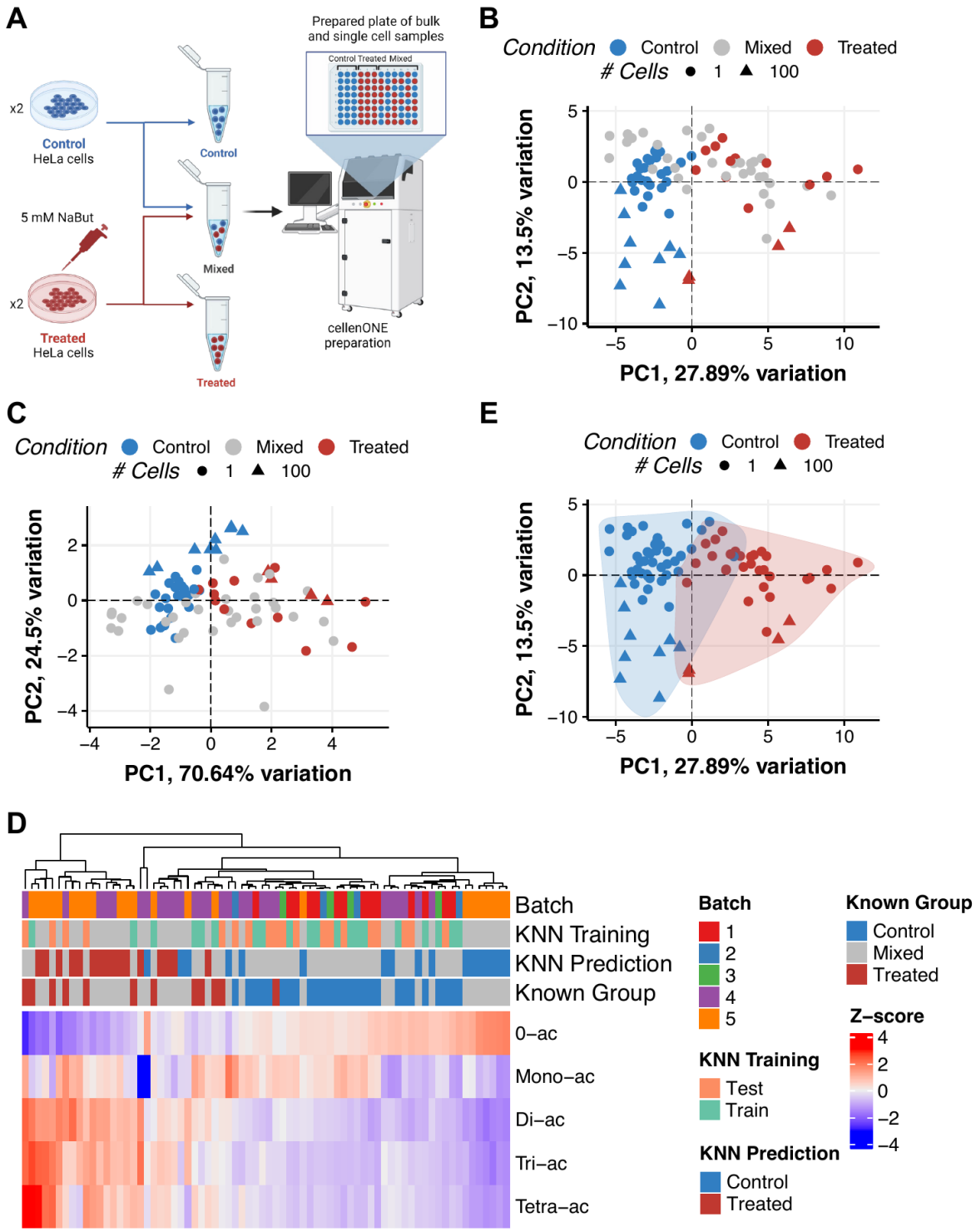

Fig. 4 | Classification of single cells following HDAC inhibitor treatment.
A) Schematic overview of experimental design where after HDAC inhibitor treatment, control and treated cell suspensions are also mixed 1:1 to create the 'mixed' group where the label of each cell is unknown. For plate layout see (**Supplementary Table 4**). **B)** Principal Component Analysis (PCA) of histone peptidoform relative abundances for single-cell and bulk (~100-cell) samples from HDAC inhibitor

experiment. Note that samples from benchmarking experiments were included to increase number of control cells, see (**Extended Data Fig. 8F**). **C)** PCA of same samples in (**B**) but instead calculated using summarized relative abundances of H4 peptide acetylation (i.e. mono, di, tri and tetra). These summarized relative abundances were then used for classifying the mixed cells into control and treated groups shown in (**D**). **D)** Heatmap and hierarchal clustering of scaled H4 peptide acetylation summarized relative abundances (Z-score) for single cells as shown in (**C**). Cells are shown in columns and H4 peptide acetylation types are shown in rows. A description of the annotation rows at the top of the heatmap (also shown in legend) starting from the 1st row and moving down to the 4th row is as follows: 1st row) batch each cell was prepared in, 2nd row) Random assignment of cells with known group (control or treated) to training (50%) and test (50%) groups to assess k-nearest neighbors (KNN) classification accuracy, 3rd row) Predicted labels of 'mixed' cells using KNN classification after training using all cells with known group, 4th row) Known group of cells used to train and test the KNN classifier, as well as validate the accuracy of the predictions. **E)** PCA, as shown in (**B**), with 'mixed' cells now classified as control or treated as predicted by KNN classification as shown in (**D**).

HDAC inhibitor treatment induces histone hyperacetylation and cell-to-cell chromatin heterogeneity

Using all known control and treated cells as well as the ones predicted by the KNN analysis (43 control and 29 treated cells in total), we next performed differential abundance analysis to assess changes in the abundance of all peptidoforms (**Methods)**. As expected, we found the majority of the acetylated peptidoforms of H1.2, H2A.1, H3 and H4 to be significantly increased in the treatment group relative to the controls (**Fig. 5A; Supplementary Tables 5-6**). The largest increase in relative abundance was observed for the tri-acetylated H4 peptidoforms, H4K5acK12acK16ac, H4K8acK12acK16ac, and H4K5acK8acK16ac. Analysis of the summarized relative abundance of each modification type (i.e. acetylation and mono-, di-, and tri-methylation representing global levels of each modification), revealed an expected significant increase in acetylation and a corresponding decrease in methylation (**Fig. 5B**). Moreover, NaBut treatment significantly increased the relative abundance of di-, tri- and tetra-acetylated H4, but not of mono-acetylated ones, indicating hyperacetylation of the H4 tail (**Fig. 5C**).

Interestingly, despite the strong nature of the NaBut treatment which leads to histone tail hyperacetylation, the relative abundance of H3 and H4 peptidoforms varied across the NaBut treated single cells (**Fig. 5D, right side**), and revealed two main subclusters, A and B (**Fig. 5E; Supplementary Table 7**). Subcluster A was characterized by low H3Kme3K14ac and H3K9me2, and hyperacetylation of H4 tails, which are associated with active transcription, whereas cells within subcluster B showed high H3Kme3K14ac and H3K9me2 and lower levels of H4 acetylation, which are associated with repressed transcription (**Fig. 5E**). This result demonstrates different

cell responses to drug perturbations and may help in understanding the mechanisms of resistance to epigenetic drugs.

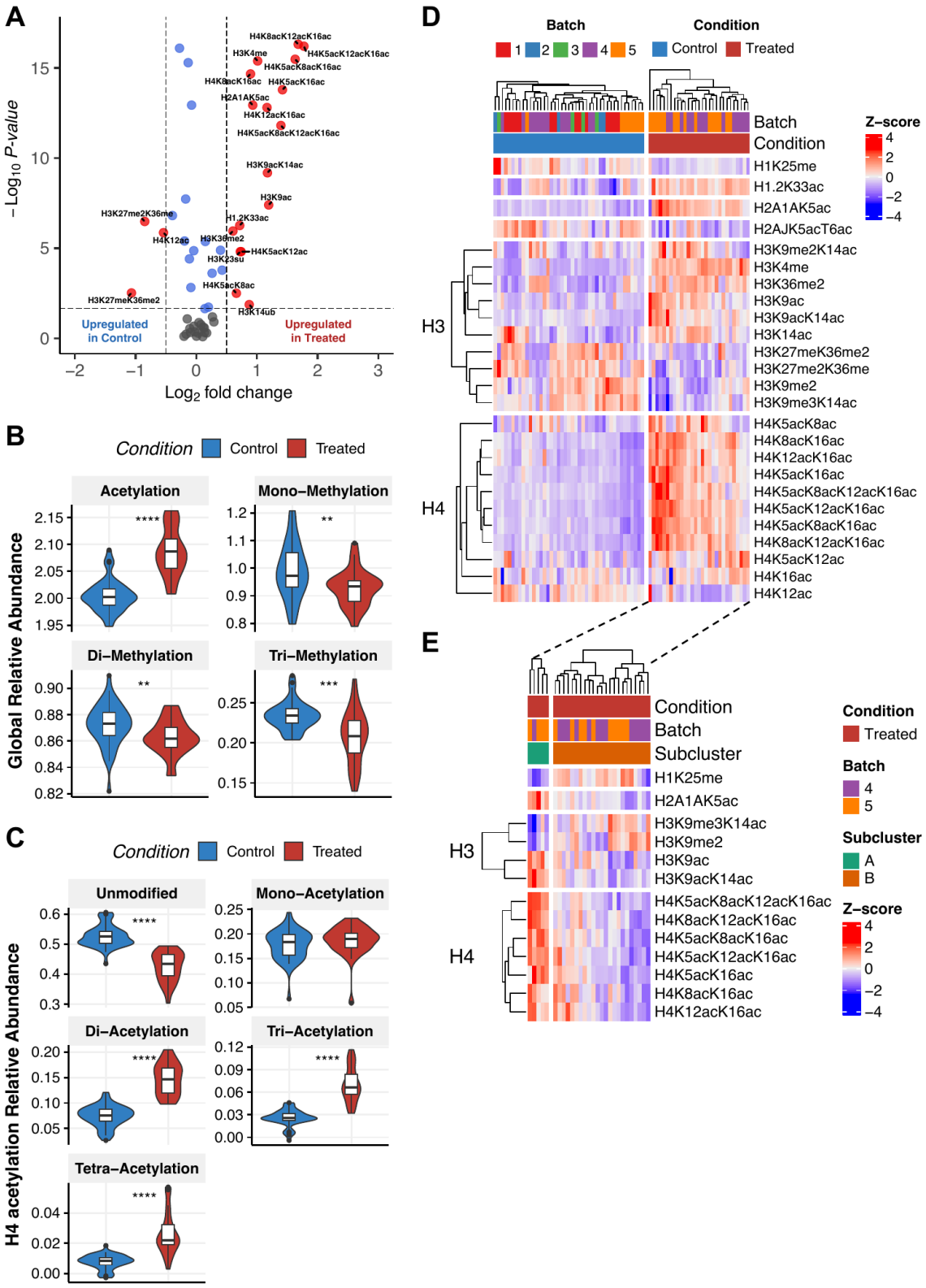

Fig. 5 | HDAC inhibitor treatment induces histone hyperacetylation and cell-to-cell chromatin heterogeneity. A) Differential abundance of modified histone peptidoforms relative abundances for single cells for treated vs. control comparison. Statistics: Wilcox test with Benjamini & Hochberg multiple testing correction. Red points are peptidoforms that are significant (adjusted p-value < 0.05) and Log_2 fold change > 0.5. Blue points are peptidoforms that are significant only. Grey points are peptidoforms that are not significant and Log_2 fold change < 0.5. For table of full results, see (**Supplementary Table 5**). **B)** Summarized relative abundances of global PTMs in single cells for treated vs. control comparison. Statistics: Wilcox test, ** p <= 0.01, *** p <= 0.001, **** p <= 0.0001. **C)** Summarized relative abundances of H4 peptide acetylation in single cells for treated vs. control comparison. Statistics: Wilcox test, ** p <= 0.01, *** p <= 0.001, **** p <= 0.0001. **D)** Heatmap and hierarchal clustering of modified histone peptidoform scaled relative abundances (Z-score) that were significantly differentially abundant (adjusted p-value < 0.05) between treated vs. control groups as shown in (**A**). Cells are shown in columns and histone peptidoforms are shown in rows. Peptidoforms are grouped by histone proteins (left side). **E)** Sub-clustering results of treated group as shown in (**D, right side**), showing 2 subclusters (A & B) of cells identified within this group and the modified histone peptidoforms that are differentially abundant (adjusted p-value < 0.1) between the subclusters. Subclusters were identified at the 2nd level of the hierarichal clustering tree shown in (**D, top-right**). Statistics: Wilcox test with Benjamini & Hochberg multiple testing correction.

Differential hPTM crosstalk induced by HDAC inhibitor treatment revealed by co-variation analysis

Cross-talk and co-regulation of hPTMs is challenging to study when hPTM abundances are averaged, such as in bulk cell workflows[42]. Thus, we leveraged the single-cell resolution of our dataset and performed co-variation analysis of hPTM abundances within the control (43 cells) and NaBut treated (29 cells) groups by correlating the relative abundances of every modified histone peptidoform to all other modified histone peptidoforms and analyzed the significant correlations (**Methods**). The resulting covariance matrix for the control group (**Fig. 6A**, **bottom-left**) was then hierarchically clustered where the resulting order of histone peptidoforms was used to order the treatment group covariance matrix (**Fig. 6A**, **top-right**). The covariance matrix of the NaBut treated cells was significantly different from that of the control cells on a global level (Mantel's test p-value=9.99*10-5), with 412 significant correlations (Two-sided T-test p-value<0.05; **Supplementary Table 8**). An increase in correlations might be expected due to higher cell-to-cell variation in the treatment group, however, this was not supported in our data as this metric was significantly lower in the treated group (**Extended Data Fig. 9A)**. In addition, the distribution of peptidoform CVs were not significantly different between the groups, indicating an equivalent amount of global epigenetic noise between the groups (**Extended Data Fig. 9B)**.

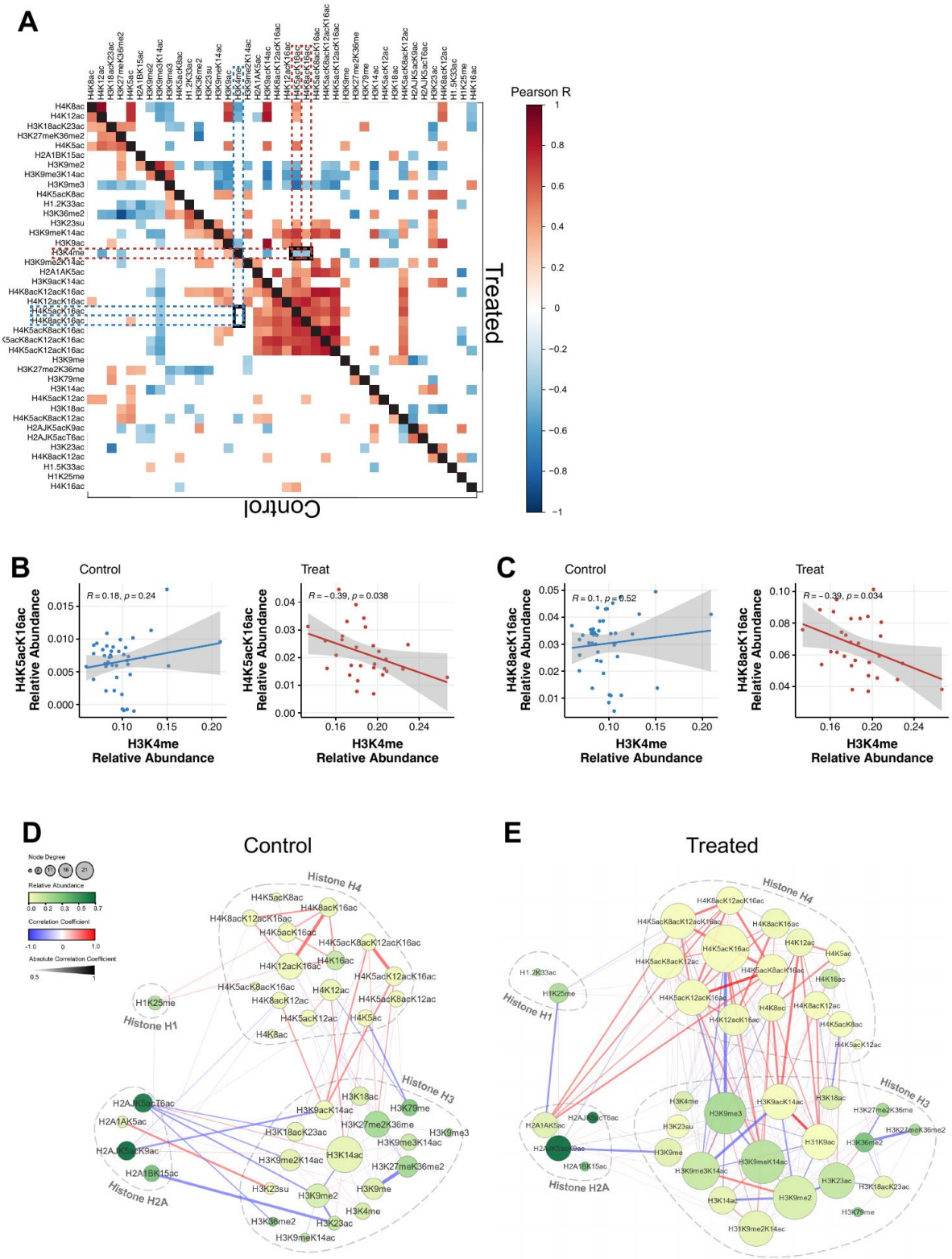

Fig. 6 | Differential hPTM crosstalk induced by HDAC inhibitor treatment revealed by co-variation analysis. A) Covariance matrix of modified histone PTM-PTM correlations derived from histone peptidoform relative abundances with significant (p-value < 0.05) Pearson R correlation coefficients shown

as colored squares. PTM-PTM correlations for control group are shown in lower-left half and upper-right half are PTM-PTM correlations for treated group. Correlations of H4K4me with H4K8acK16ac and H4K4me with H4K5acK16ac, which are significantly altered due to NaBut treatment (adjusted p-value < 0.05), are highlighted in the control (blue dashed outline) and treated (red dashed outline) groups. Statistics: Significance of Pearson R correlation coefficients was tested using Pearson's product moment correlation coefficient; Significance of differential Pearson R correlation coefficients was tested using a permutation test with 10,000 permutations. For a table of Pearson R correlation coefficients p-values, see (**Supplementary Table 8**). For full results and table of differential Pearson R correlation coefficient testing, see (**Extended Data Fig. 9C and Supplementary Table 9**). **B-C)** Comparison of histone peptidoform relative abundances in single-cells for PTM-PTM correlations which were significantly altered due to NaBut treatment highlighted in (**A**). Correlations of H4K4me with H4K5acK16ac are shown in (**B**) and correlations of H4K4me and H4K8acK16ac are shown in (**C**). Within each panel, the control group is shown on left subpanel and treated on right subpanel. Statistics: Pearson R correlation coefficients were tested using Pearson's product moment correlation coefficient. **D-E)** Network diagrams derived from covariance matrices shown in (**A**), showing the significant Pearson R correlation coefficients of modified histone PTM-PTM correlations (edges) for each of the modified hPTMs (nodes). Control group shown in (**D**) and treated in (**E**). Node size represents node degree (i.e. number of significant correlations), node color represents mean relative abundance amongst all cells in control and treated groups, edge color represents absolute correlation coefficient, and edge width represents the scaled correlation coefficient.

To assess differential PTM-PTM correlations, which may reveal biological shifts in the co-regulation of hPTMs, we compared the covariance matrices between the treatment and control groups and calculated p-values through bootstrapping (**Extended Data Fig. 9C; Methods; Supplementary Table 9**). Globally, there was a shift towards more significant positive correlations in the treated group, indicating a higher degree of synchronous co-regulation in response to the Nabut treatment (**Extended Data Fig. 9D**). In the control group, a group of hPTMs, encompassing acetylations associated with open chromatin and gene expression[3] (i.e. H4K8acK12acK16ac, H4K1212acK16ac, H4K5acK16ac, H4K8acK16ac, H4K5acK8acK16ac, H4K5acK8acK12acK16ac, and H4K5acK12acK16ac), had significant positive correlations with each other, as would be expected (**Fig. 6A**, **bottom-left**). In contrast, the bivalent hPTM H3K9me3K14ac, associated with a poised chromatin inactive state[43], negatively correlated with the aforementioned acetylated peptidoforms, in addition to H2A1AK5ac, H3K9acK14ac, and H3K9me (**Fig. 6A**, **bottom-left**). In the treated group, the most notable change due to HDAC inhibition was a significant decrease in the correlations of H3K4me with H4K8acK16ac and H3K4me with H4K8acK16ac (**Figs. 6A top-right, and 6B-C)**. These negative correlations were absent in the control group (**Fig. 6A intersection of dotted lines, Extended Data Fig. 9C**). This was an unexpected finding given that H3K4me, H4K8acK16ac, and H4K8acK16ac were amongst the most significantly upregulated peptidoforms upon HDAC inhibitor treatment (**Fig. 5A**).

To gain a different perspective of hPTM cross-talk, we visualized the PTM-PTM correlations of the control and treated groups as network graphs (**Fig. 6D-E)**. This clearly revealed patterns of regulation between hPTMs within the same histone tail (intra-) as well as those across histone tails (inter-). For example, in the control group, there is a lack of intra-H2A PTM correlations. Instead, relatively strong inter-H2A-H3 PTM correlations can be seen, such as the positive relationship of H2AK5ac with H3K23su (**Fig. 6D, lower-left)**. In addition, highly connected hubs of hPTMs in the treated group, such as H4K5acK16ac or H3K9meK14ac, can be seen in the treated group (**Fig. 6E, top-right)** which may represent hPTMs central to the epigenetic regulatory network and could be crucial points for intervention.

Discussion

This study presents a novel MS-based workflow that enables accurate and comprehensive profiling of hPTMs at single-cell resolution. We successfully identified 68 histone peptidoforms encompassing 25 individual hPTMs of which 46 were characterized sufficiently confident for quantification and downstream analyses. Comparatively, in bulk histone analysis via LC-MS/MS, approximately 200-300 histone peptidoforms are typically identified[26,36,39,44]. Our workflow constitutes a significant advance over previous antibody-based single-cell epigenomic approaches, which are limited in the number of targets and prone to cross-reactivity. Moreover, our methodology enables the identification and quantification of less common PTMs beyond currently available antibodies (i.e. H3K23 succinylation) or previously unrecognized modifications, (i.e. histidine methylation on H2A)[45].

A key strength of our method is the ability to detect co-occurring histone modifications, or "combinatorial histone marks", on the same peptide. Such combinatorial hPTM patterns are thought to play a crucial role in establishing distinct chromatin states and recruiting chromatin-modifying enzymes. This proves particularly valuable for aging studies, given the bivalent chromatin domains like H3K4me3 and H3K27me3 in stem cells[4]. However, accurate quantification of combinatorial hPTM from bulk samples is challenged by cell-to-cell heterogeneity. We here demonstrate that histone codes such as H3K9me2K14ac and H3K9me3K14ac are relatively abundant, indicating that we can potentially quantify cell-to-cell heterogeneity of chromatin domains decorated by silencing heterochromatin marks but may still be accessible due to acetylation. The high variation of H3K9me3 is likely due to its known role in chromatin condensation during mitosis as cells in these experiments did not have their cell cycle synchronized. On the other hand, the lack of variation in H2AJK5acK9ac is a novel finding as this combinatorial modification on a variant of the H2A histone is poorly studied and may represent a stable epigenetic modification in proliferating cells in culture. Such insights into the cell-to-cell variability of the epigenetic landscape have important implications for understanding mechanisms of cellular proliferation, differentiation, adaptation, disease progression, and aging.

Furthermore, we demonstrated the utility of our method in detecting co-regulations of hPTMs in response to the HDAC inhibitor sodium butyrate. We were able to clearly distinguish treated from untreated cells and observed considerable changes in the cell-to-cell co-regulation, in particular for acetylations (**Fig. 6**). This differential hPTM crosstalk could suggest an inhibitory effect of hyperacetylation in particular on histone H4 by altering the chromatin structure and reducing its accessibility also for methylating enzymes. It should be noted that with the analysis of hPTMs

which vary from cell-to-cell (**Fig. 3F**), the most variable hPTMs will reflect the underlying variability of cell states. On the other hand, the analysis of the covariance of hPTMs is not reflective of this, even though it relies on subtle variation of hPTM levels from cell-to-cell. Consequently, while individual hPTMs may exhibit high variability due to cell cycle effects in our model system, covariance analysis can reveal regulatory relationships and functional interactions between hPTMs that are independent of cell cycle stage. This allows us to identify sets of hPTMs that may be co-regulated or functionally linked, providing insights into the coordinated regulation of chromatin states beyond cell cycle-dependent changes.

We also identified potential areas of improvement of our method, including enhancing the digestion and derivatization efficiency. In fact, in contrast to traditional bulk analysis we bypassed histone extraction to avoid the risk of losing individual cells. This led to a non-complete production of expected peptides (**Supplementary Figs. 2A-D**). In addition, we expect that a characterization of the proteome beyond histone proteins is achievable from the same spectra. This dual-purpose approach holds promise for enhancing the comprehensiveness of our analysis, offering insights into broader cellular processes and their correlation to the respective histone code. In a recent development, a standard SCP workflow successfully identified 16 histone modification sites in single H358 cells[46,47]. Despite the lower histone coverage upon trypsin digestion compared to ArgC, this paves the way for other researchers to explore hPTMs in their own SCP datasets. Furthermore, in future studies we aim to enhance the throughput of the analysis by optimizing the chromatographic separation and employ a targeted MS acquisition strategy, such as parallel reaction monitoring (PRM) on the Bruker timsTOF instruments (prmPASEF)[28,48]. We expect that very short gradients, e.g. 5 min, are feasible to maintain similar sensitivity and potentially achieve the analysis of hundreds of cells per day.[28,48].

Finally, given the intricate combinatorial complexity of the histone code, allowing for billions of combinations of post-translational modifications (PTMs), peak picking and data processing still requires manual refinement. This is especially due to identical mass shifts of certain PTMs that result in isobaric forms (e.g. identical peptide sequences with the same type of PTM on different amino acids). In contrast to conventional bulk histone analysis (i.e. millions of cells), some isobaric peptidoforms separate in retention time. This is likely attributed to the reduced loading of the sample resulting in sharper chromatographic peaks. Nevertheless, certain peptidoforms still co-elute, necessitating deconvolution through a combination of unique fragment ions (**Extended Data Fig. 2**). The comprehensive and reproducible fragmentation patterns generated with DIA enables the relative comparison of those across large sample numbers. However, at present, only

a limited number of tools can effectively process histone DIA data, including Skyline and EpiProfile[34]. The development of dedicated computational tools tailored for the analysis of histone diaPASEF data will therefore be an important step towards accessibility of this approach.

In conclusion, this study presents a robust and versatile MS-based workflow to profile the histone code at single-cell resolution. We provide unprecedented insights into the epigenetic heterogeneity within cell populations and we hope to open new avenues for investigating the role of the histone code in diverse biological processes and diseases.

Extended Methods

Cell culture – Low passage HeLa cells (ATCC CCL-2), were grown as adherent cultures in Eagle's Minimum Essential Medium (ATCC 30-2003) supplemented with 10% fetal bovine serum (Thermo A5256801) and 1% penicillin-streptomycin (Thermo 15140122) in 10 cm dishes (Thermo 172931) at 5% CO_2 and 37°C. Cells were passaged at 70-80% confluence every 3 days. For drug treatment studies, fresh media was supplemented with either 1X PBS (Thermo 10010023) as a vehicle control or sodium butyrate (Sigma-Aldrich 303410) at a concentration of 5 mM. The treatment was administered for 24 hours, after which the cells were harvested for single-cell isolation and downstream sample preparation.

Cell isolation – Prior to harvesting, cells were washed with ice-cold 1X PBS. Cell detachment was achieved by treating the cells with 1 mL of trypLE (Thermo 12604013), followed by incubation at 37°C for 3-5 min. Post-detachment, the cells were washed with ice-cold 1X PBS and then centrifuged at 500G for 5 min at 4°C. The resultant cell pellet was resuspended in ice-cold 1X PBS. The suspension was strained using a 40 µm cell strainer (Millipore Sigma CLS431750), followed by an additional round of centrifugation and washing. Cell concentration was determined using a Countess™ 3 Automated Cell Counter (Fisher AMQAX2000) to obtain a suspension of 200 cells/µL. Cells were kept on ice prior to cell sorting.

Single-cell isolation and histone peptide preparation – Reagents were prepared fresh on the day of sample processing. The cellenONE instrument (Cellenion) was prepared by degassing the system water, performing a system prime, and confirmation of a stable drop. A type 1 piezo dispense capillary (Cellenion piezo dispense capillary; PDC) was used for cell sorting and liquid handling. All steps performed outside of the cellenONE were done in a sterile cell culture hood with laminar air flow. Custom programs were created for the cellenONE instrument for each step of the process (see ‘Code Availability’). 384-well plates (Thermo AB1384) were used for cell isolation and histone preparation and were prepared beforehand by dispensing 1 µL of lysis reagent (0.2% dodecyl maltoside Thermo 89902 in 1M TEAB Millipore Sigma 18597) to appropriate wells using an electronic multichannel pipette (Sartorius LH-747321) and then placed in a 384-well plate holder in the cellenONE instrument that was chilled to 4°C. A 1 pg/nL bovine histone standard (Sigma-Aldrich H9250) suspension in 1X PBS was degassed on ice for 10 min, 20 µL was then loaded into the piezo dispense capillary (PDC) of the cellenONE instrument, and

then various amounts of the histone standard (i.e. 10, 20, 40, 80, and 100 pg) were distributed to specified wells using the 'Reagent_Dispense' program (**Supplementary Table 2**). Following this, the plate was sealed (Thermo AB0626), vortexed for 5 sec, and centrifuged at 500 G for 30 sec. To filter out dead cells during cell sorting, DAPI stain (Thermo D1306) was added to the cell suspension prior to sorting at a concentration of 1 µg/mL, followed by degassing on ice for 10 min. 20 µL of the cell suspension was then loaded into PDC of the cellenONE and the cellenOne module was used to perform analysis and set the gating based on cell size, circularity, and DAPI detection. Live single-cells were then sorted into the wells of the plate using the 'cellenONE_Basic_WithscanFields' program where images of each isolated cell were acquired to verify successful isolation (**Supplementary Figs. 1A-D**). Successful isolation was also confirmed by acquiring images of single-cells that were isolated into wells that contained no reagents in the last row of each column on the plate. Following this, 100-cell bulk samples were created by resuspending the cell suspension in lysis reagent at a concentration of 100 cell/µL and manually dispensing 1 µL into the specified wells (**Supplementary Table 2**). Following this, 100-cell bulk samples were prepared identically to single-cell samples. The plate was then sealed, vortexed for 5 sec, and centrifuged at 500 G for 30 sec.

Following cell isolation and lysis, histone preparation begins with the 1st round of derivatization where 10X propionylation reagent (25% propionic anhydride Sigma-Aldrich 240311 and 75% acetonitrile Sigma-Aldrich 34851) was degassed on ice for 10 min and then 10 µL was loaded into PDC of the cellenONE. Nozzle parameters, i.e. voltage, pulse, and delay (400 ms), were tuned to account for low viscosity of the propionylation reagent to obtain a stable drop (**Supplementary Fig. 1E**). The 'Derivatization_Dispense' program was then used to dispense 100 nL of propionylation reagent to obtain a final concentration of 1X in each well. The plate was then sealed, vortexed for 5 sec, and centrifuged at 500 G for 30 sec. Images of wells were acquired to confirm successful reagent dispense (**Supplementary Figs. 1F-G**). The plate was then incubated at RT for 30 min, followed by drying inside of the cellenONE for 10-15 min with the plate holder heated to 50°C. Following this, 1 µL of master mix reagent (100 ng/µL Trypsin Gold Promega V5280, 10 U/µL Benzonase® Nuclease Millipore E1014, 1% ProteaseMAX™ Promega V2071, 1 M TEAB) was dispensed into wells using a electronic multichannel pipette. The plate was then sealed, vortexed for 5 sec, and centrifuged at 500 G for 30 sec. The sealed plate was placed back into the cellenONE where the 'Digestion_Incubation' program was run which incubates the plate for 2 hr with the plate holder heated to 50°C. Following the incubation, the plate was centrifuged at 500 G for 30 sec to pull down any condensation. The plate was then placed back into the cellenONE where the 2nd round of derivatization was performed that is

identical to the 1st round as described above. Finally, derivatized and digested histone peptides were diluted by dispensing 2.9 µL of dilution solution (0.1% Trifluoroacetic acid Sigma-Alrich T6508, 5% DMSO Thermo 85190, mass spec grade H_2O Sigma-Alrich 900682) into wells using a electronic multichannel pipette. The plate was then sealed, vortexed for 5 sec, and centrifuged at 500 G for 30 sec. Prepared plates were stored at -80°C until ready for LC-MS analysis.

LC-MS/MS analysis – Samples were analyzed using a Vanquish Neo UHPLC system (Thermo Fisher Scientific) coupled to a timsTOF Ultra (Bruker Daltonik Gmbh). Peptides were separated on an Aurora Ultimate (25 cm x 75 µM, 1.7 µm particle size and 120 Å pore size IonOpticks AUR3-25075C18-CSI) integrated emitter column and eluted over a 30-minute window using the following gradient: 5-23% Solvent B (0.1% formic acid Sigma-Aldrich F0507, acetonitrile) in 25.7 minutes, 23-35% Solvent B in 2.6 minutes and 35-45% Solvent B in 1.7 minutes, at a flow rate of 200 nL/min. For shorter chromatographic gradients, peptides eluted either over a 10-minute window ranging from 5-23% Solvent B in 5.8 minutes and 23-45% Solvent B in 4 minutes or over a 5-minute window ranging from 5-45% Solvent B in 4.8 minutes. The actively acquired sample plate was stored in the Vanquish Neo autosampler at 7°C. To minimize evaporation, samples for 12 hours of measurement time were unsealed at a time and the entire sample volume was injected for every analytical run.

For dda-PASEF experiments, full MS data were acquired in the range of 100-1700 m/z and 1.6 1/K0 [V-s/cm^{-2}] to 0.6 1/K0 [V-s/cm^{-2}]. Precursors were isolated with 2 m/z at 700 m/z or 3 m/z at 800 m/z. For dia-PASEF, full MS data were acquired in the range of 100-1700 m/z and 1.3 1/K0 [V-s/cm^{-2}] to 0.6 1/K0 [V-s/cm^{-2}]. DIA windows ranged from 300 m/z to 1000 m/z with 30 Th isolation windows and were acquired with ramp times of 200 ms. High sensitivity detection for low sample amounts was enabled without dia-PASEF data denoising. For both dia- and ddaPASEF the collision energy was ramped as a function of increasing mobility starting from 20 eV at 1/K0 [V-s/cm^{-2}] to 59 eV at 1.6 1/K0 [V-s/cm^{-2}].

Histone peptide identification and quantification – Peptide identification and quantification was performed using Skyline v22.2 as previously described[12]. Briefly, ArgC was used as the digestion enzyme due to peptide derivatization. Charge states 1+ and 2+ were considered for precursor ions, and charge states 1+ and 2+ were considered for product ions. All sidechain modifications were set as variable modifications and a maximum of four modifications were allowed to occur on

any peptide. Propionyl on K and the N-terminus were set as fixed. Importantly, Skyline only allows one modification per amino acid. However, when a peptide starts with a K, there can be both a propionyl on the N-terminus and a variable modification on the side chain. Therefore, new modifications were made in Skyline by combining the mass of propionyl groups with all possible side chain modifications. Next, a FASTA database containing all histone variants was imported to complete the target library in Skyline. This target list was further complemented by adding all possible modified histone ArgC peptides as previously described[13]. Shared peptides between different histone variants were allocated to the first occurring protein. The staggered windows used for diaPASEF acquisition as described above were set as the isolation scheme. Raw diaPASEF data of the 100-cell and 100 pg histone standard samples was imported into Skyline and all peptides in the target list were manually curated and used as a reference for single-cell samples. This was done based on the alignment of MS1 and MS2 XICs, relative retention time differences expected between unmodified and modified peptides, and filtering for unique transitions (if applicable). Peptides that could not be confidently identified were flagged and filtered out for further analysis. This Skyline project was then used to create a spectral library to facilitate peak picking for single-cell samples. A separate Skyline project was made for every batch, where these all used the same target list and manually curated spectral library. Following this, raw diaPASEF data of single-cells was imported into Skyline, peak picking was facilitated by limiting scans to within 2 minutes of the MS/MS ID in the spectral library with manual adjustment if needed. Peaks for each peptide in single-cell samples were then validated if no peak was detected in the empty well samples and the peak aligned with the histone standard and the 100-cell samples. Finally, the results were exported in CSV format including total MS1, fragment Area, retention time, and precursor charge for all peptides in every sample. All curated skyline projects are accessible through the Panorama database, including spectral libraries (see 'Data Availability').

Isobaric peptide deconvolution – Histone H4 contains isobaric peptides which could not be separated by liquid chromatography (**Supplementary Fig. 3A**). Thus, we deconvoluted the MS1 signal intensity using a combination of unique fragment ions for each peptidoform (**Supplementary Fig. 3B**) as has been previously described[34]. First, for each of the isobaric peptides, the fragment ion intensity was summed for all the fragment ions, the unique fragment ions, and the fragment ions that created a unique combination (unique combination fragment ions). Second, the proportion of the isobaric peptide with unique fragments is obtained by taking

the proportion of unique fragments relative to all the fragments. Third, the proportion of all the remaining isobaric peptides (which have unique combination fragment ions) is obtained by subtracting the proportion of the isobaric peptide with unique fragments from 1. Fourth, to get the relative proportion of each of the remaining isobaric peptides, the proportion of the unique combination fragment ions relative to all the fragment ions for that peptide is divided by the sum of the unique combination fragment ions for all the remaining isobaric peptides. Fifth, to get the proportion of each of the remaining isobaric peptides (which have unique combination fragment ions), the relative proportion of each of these peptides is multiplied by the proportion of all the remaining isobaric peptides obtained in the third step. Sixth, the proportion of all the isobaric peptides is summed and checked to be equal to 1. Finally, the convoluted MS1 signal for isobaric peptides is multiplied by the proportion of isobaric peptides obtained in the fifth step which results in the deconvoluted MS1 signal for each isobaric peptide. These calculations can be expressed as the following set of equations:

For a set of n isobaric peptides (P1, P2, ..., Pn), where P1 has unique fragments and P2 to Pn have a unique combination of fragments:

$$MS1_{deconvoluted}(P_i) = MS1_{original} \cdot Prop(P_i)$$

Where:

$$Prop(P1) = \frac{UF(P1)}{TF(P1)}$$

Thus, for *i* = 2 to *n*:

$$Prop(P_i) = (1 - Prop(P1)) \cdot \frac{\frac{UCF(P_i)}{TF(P_i)}}{\sum_{j=2}^{n} \frac{UCF(P_j)}{TF(P_j)}}$$

Given:

$MS1_{original}$ = Original (convoluted) MS1 signal

$MS1_{deconvoluted}(P_i)$ = Deconvoluted MS1 signal for peptide *i*

$Prop(P_i)$ = Proportion of signal attributed to peptide *i*

$UF(P_i)$ = Sum of unique fragment intensities for peptide *i*

$UCF(P_i)$ = Sum of unique combination fragment intensities for peptide *i*

$TF(P_i)$ = Sum of all fragment intensities for peptide *i*

Derivatization efficiency analysis – A Skyline project was created with a target list being different variations of the unmodified H3.1 9-17 peptide that represented the fully propionylated peptide (ArgC-like peptide with propionyl modifications at K and N-terminus), the non-propionylated peptide (Tryptic peptide with 1 or 2 missed cleavages), under-propionylated in the 1st round of derivatization (Tryptic peptide with 1 missed cleavage and propionyl modifications at K and N-terminus), under-propionylated in the 2nd round of derivatization (ArgC-like peptide with propionyl modifications at K) and over-propionylated (ArgC-like peptide with propionyl modifications at T)[49]. Following this, raw diaPASEF data of single-cells and 10 pg histone standards from the first batch were imported into Skyline and the raw MS1 intensity was analyzed.

Peptide filtering – Peptides where only the unmodified form was detected were removed. For peptides with multiple precursor charges (i.e. +2 and +3 for H3K4un and H3K4me), those with the lower median MS1 signal intensity across all cells in the analysis were removed. Peptides which were not detected in greater than 50% of cells were considered unreliable and were removed. Peptides with less than 120% the median MS1 signal intensity in single-cell samples relative to empty samples were considered to be background noise and were removed (**Extended data Fig. 2A, red stars**). Peptides with a median correlation of less than R=0.8 or insignificant correlation (p-value > 0.05) derived from the titration curve analysis were considered to be unsuitable for quantification and were removed (**Extended data Fig. 3B, red stars**).

Cell filtering – Based on MS1 signal distributions of peptides for each single-cell sample, samples whose MS1 signal distribution was 1 median absolute deviation lower than the global median intensity were considered to be sample preparation failures and were removed. This threshold was set based on the MS1 signal distribution of empty samples.

Peptide Ratio Normalization – For each peptide that contained at least 1 modified form, the peptide ratio was calculated for each of the peptidoforms by normalizing the MS1 intensity signal by the sum of the MS1 intensity signals of all the peptidoforms that shared the same peptide sequence (e.g. for H2A1 4-11, H2A1K5unK9un and H2A1K5acK9un were used to create the peptide ratio). Following this peptide ratios are Log(1 + *x*) transformed to account for the left-skewed distribution inherent to ratio data. Single PTM ratios were calculated by summing the

peptide ratios for every unique modification at each amino acid in a peptide (e.g. H3K9ac = H3K9acK14un + H3K9acK14ac) . Global PTM ratios were calculated by summing the single PTM ratios for each of the unique modifications (e.g. ac = H3K9ac + H3K14ac + H4K8ac…etc.). The summarized H4 acetylation PTM ratios were calculated by summing the peptide ratios of peptides containing 1 (mono), 2 (di), or 3 (tri) acetylation modifications (e.g. mono = H4K5acK8unK12unK16un + H4K5unK8acK12unK16un + H4K5unK8unK12acK16un + H4K5unK8unK12unK16ac).

Batch Correction – The presence of a batch effect was assessed by the qualitative analysis of PCA plots of the first 2 principal components by identifying a significant correlation of these to the variable encoding the batch (e.g. **Extended Data Fig. 5A**). The removeBatchEffect function from the limma package[50] was then used to adjust the peptide ratios to account for the batch effect while preserving the effect encoded in experimental variables (i.e. treated and untreated).

Single-cell vs. bulk comparisons – ~100-cell bulk and single-cell samples from batches 1-3 were processed as described above. To compare histone peptide ratio between single-cell and 100-cell bulk samples, the mean histone peptide ratio (pseudobulk) was calculated across the single-cells and correlated to the histone peptide ratio of the 100-cell bulk samples. To compare raw MS1 signal between single-cell and 100-cell bulk samples, the MS1 signal (pseudobulk) was summed across the single-cells and correlated to the MS1 signal of the 100-cell bulk samples. To calculate the Log_2 fold change of each peptide between single-cell and 100-cell bulk samples, the peptide ratio for each peptidoform in each cell was compared to the mean histone peptide ratio of 100-cell bulk samples across all batches. PCA of single-cell and 100-cell bulk samples was performed using the PCAtools package[51] on normalized and batch-corrected histone peptide ratios that were centered and scaled. Single PTM ratios were calculated for single-cell and 100-cell bulk samples as described above.

Technical and biological noise analysis – To analyze technical noise, histone standard samples from batches 1-3 were processed identically to single-cell samples as described above. The coefficient of variation (CV) of the normalized and batch-corrected histone peptide ratio was calculated for histone standard samples within each batch (intra-) or across batches (inter-). The CV of the normalized histone peptide ratio without batch-correction was also calculated.

For comparison of technical variability derived from histone standards to external datasets, histone peptide ratio data of HeLa cell derived bulk technical replicates (Sidoli et al., 2015 A[30,38,39], 5 replicates, 16 peptidoforms; Sidoli et al., 2015 B[30,38,39], 4 replicates, 12 peptidoforms) was obtained from the supplementary data. In addition, level 3 normalized data (Light(PTM)/Heavy(PTM) divided by Light(NORM)/Heavy(NORM)) of processing replicates for cell lines in the NIH Library of Integrated Network-Based Cellular Signatures consortium (Dele-Oni et al., 2021[30,38,3940], 3 replicates, 29 peptidoforms) was downloaded from Panorama (https://panoramaweb.org/lincs_pccse_gcp_2020.url). For both external datasets, peptidoforms were matched to those identified in histone standard samples across all batches. The CV was then calculated for the matched peptidoforms of the technical replicates in the external datasets and compared to the inter-batch CV derived from matched peptidoforms of the histone standards in the current dataset.

To analyze biological (cell-to-cell) noise, single-cell samples from batches 1-3 were processed as described above to obtain normalized and batch-corrected histone peptide ratios. Following this, the CV of modified peptidoforms was calculated by taking the CV of each modified peptidoform across all single-cells in all batches, resulting in biological + technical noise. To adjust for technical noise, we assume that the total observed noise is the sum of the technical and biological noise. First, the variance of each peptidoform derived from the 10 pg histone standards (technical noise) is subtracted from the variance of each peptidoform derived from the single-cell samples (biological + technical noise) to obtain the adjusted biological variance for each peptidoform. Second, the square root of the adjusted biological noise of each peptidoform is divided by its respective mean to obtain the adjusted biological CV. Peptidoforms where the technical variance was greater than the biological + technical variance were discarded.

Cell classification analysis – Single-cells from batches 1-3 (22 control single-cells) and batches 4 and 5 (9 control, 16 treated, 33 mixed single-cells) were processed as described above to obtain normalized and batch-corrected histone peptide ratios. PCA of single-cells was performed using the PCAtools package[51] where histone peptide ratios were centered and scaled. Following this, summarized H4 acetylation PTM ratios were calculated as described above and PCA was performed on these scaled and centered summarized ratios (Z-scores). The heatmap of scaled and centered summarized ratios (Z-scores) was plotted using the ComplexHeatmap package where hierarchical clustering was performed on the summarized H4 acetylation PTMs (rows) and single-cells (columns)[52]. To classify cells in the mixed group as belonging to the control or treated

groups, we trained and evaluated a K-nearest-neighbors (KNN) classifier based off of the scaled and centered summarized ratios (Z-scores). To evaluate the KNN classifier, cells from the control and treated groups were randomly split 50:50 into training and test groups where k = 2. Following this, all cells from the control and treated groups were used for training to predict the labels of cells from the mixed group. The predicted labels (control or treated) of cells in the mixed group were then used in the downstream analyses.

Differential abundance analysis – ~100-cell bulk and single-cell samples from batches 1-5 were processed as described above to obtain normalized and batch-corrected histone peptide ratios. Predicted labels of cells originated from the mixed group in batches 4 and 5 were used to increase the number of cells in the control and treated groups. For ~100-cell bulk samples, differential abundance of modified peptidoforms (4 treated vs 9 control) was performed using an unpaired two-sided T-test followed by Benjamini-Hochberg multiple hypothesis correction. For single-cell samples, differential abundance of modified peptidoforms (29 treated vs 43 control) was performed using an unpaired Wilcoxon rank sum test followed by Benjamini-Hochberg multiple hypothesis correction. Log_2 fold changes were calculated using the median values of each peptidoform for each group. The heatmap of scaled and centered histone peptide ratios (Z-scores) of significant peptidoforms (adjusted p-value < 0.05 and Log_2 fold change > 0.5) was plotted using the ComplexHeatmap package where hierarchical clustering was performed on the peptidoforms (rows) and single-cells (columns)[52]. Differential abundance of single-cell global PTM relative abundances and summarized H4 acetylation PTM relative abundances were performed using an unpaired Wilcoxon rank sum test.

Sub-clustering analysis – Following differential abundance analysis, the significant peptidoforms (adjusted p-value < 0.05) resulting from the treated vs control comparison were subsetted along with the cells from the treated group. Following this, hierarchical clustering was performed on the scaled and centered histone peptide ratios (Z-scores) to cluster histone peptides (rows) and single-cells (columns). 2 subclusters were identified at the 2nd level of the hierarchical clustering tree which were labeled ‘A’ and ‘B.’ Differential abundance analysis differential abundance of modified peptidoforms (6 subcluster A vs 23 subcluster B) was performed using an unpaired Wilcoxon rank sum test followed by Benjamini-Hochberg multiple hypothesis correction. Log_2 fold changes were calculated using the median values of each peptidoform for each group. The heatmap of scaled and centered histone peptide ratios (Z-scores) of significant peptidoforms

(adjusted p-value < 0.1) was plotted using the ComplexHeatmap package where hierarchical clustering was performed on the peptidoforms (rows) and single-cells (columns)[52].

PTM-PTM co-variation analysis – Single-cell samples from batches 1-5 were processed as described above to obtain normalized and batch-corrected histone peptide ratios. For each group (29 treated and 43 control) and all modified peptidoforms, a covariance matrix was calculated by obtaining Pearson R values and p-values of each PTM-PTM correlation were calculated using a two-sided T-test. The lower triangle of each covariance matrix was visualized using the corrplot package[53] where only significant (p-value < 0.05) are shown. Covariance matrices were then filtered on significance (p-value < 0.05) and parsed into a long format using a custom R script. Network diagrams were made using Cytoscape. Comparison of treated vs control covariance matrices was performed using Mantel's permutation test with 10,000 permutations. Comparison of PTM-PTM correlations between treated vs control covariance matrices was performed using a permutation test with 10,000 permutations followed by Benjamini-Hochberg multiple hypothesis correction. $\text{Log}_2(x + 1)$ fold changes comparing PTM-PTM correlations between treated vs control were also calculated and visualized as a histogram. Scatter plots of peptidoform relative abundance for specific PTM-PTM relationships were fit using a linear model. In addition, Pearson R correlation coefficients and p-values of the correlations were calculated using a two-sided T-test.

Cell-cell variation analysis – Single-cell samples from batches 1-5 were processed as described above to obtain normalized and batch-corrected histone peptide ratios. For each group (29 treated and 43 control) and all modified peptidoforms, the pairwise Euclidean distance between all cells within each group was calculated and then compared using an unpaired T-test. Following the same procedure, the CV within each group was calculated and then compared using an unpaired T-test.

Data availability

The raw mass spectrometry-based proteomics data generated in this study have been deposited in the MassIVE database under accession code MSV000094801 [https://massive.ucsd.edu/ProteoSAFe/dataset.jsp?accession=MSV000094801]. The data is

currently accessible with the password: schPTM and will be made publicly available after publication.

Code availability

All analysis scripts to process data and re-create figures are available at: https://github.com/cutleraging/single-cell-histone-ptm

Acknowledgements

We thank all members of the Sidoli and Vijg laboratories for helpful discussions. C.C. is a recipient of a SPARC Award from the Broad Institute of MIT & Harvard (#800444) that partially supported this work. L.C. acknowledges the Research Foundation Flanders – FWO for personal funding (1SF2622N) and awarding a mobility grant to join the Sidoli Lab (V400623N). This work has been supported in part by grants: T32AG023475 to R.C.; U19AG056278, U01HL145560, U01ES029519, P01AG017242, P01AG047200, RF1AG068908, P30AG038072, US Department of Defense (BC180689P1) to J.V.; P01CA206978, U24CA270823, U01CA271402 to S.A.C. This work was also supported by the Michael J. Fox Foundation and the Paul F. Glenn Center for the Biology of Human Aging at Albert Einstein College of Medicine. The Sidoli lab gratefully acknowledges for funding the Hevolution Foundation, the Einstein-Mount Sinai Diabetes center, Merck, Relay Therapeutics, and the NIH Office of the Director (S10OD030286).

Author contributions

R.C. and S.S. conceptualized and designed the experiments. R.C., L.C., and J.C., designed the sample preparation method and prepared the samples. C.C. acquired the samples. R.C., L.C., and C.C. analyzed the data and wrote the manuscript. D.D. acquired funding. S.A.J.V., M.D., M.P., S.A.C., J.V., and S.S. supervised the research and revised the manuscript.

Conflicts of interest

S.A.C. is a member of the scientific advisory boards of Kymera, PTM BioLabs, Seer and PrognomIQ.

References

1. Bernstein, B. E., Meissner, A. & Lander, E. S. The mammalian epigenome. *Cell* **128**, 669–681 (2007).
2. Jenuwein, T. & Allis, C. D. Translating the Histone Code. *Science* **293**, 1074–1080 (2001).
3. Shogren-Knaak, M. *et al.* Histone H4-K16 acetylation controls chromatin structure and protein interactions. *Science* **311**, 844–847 (2006).
4. Bernstein, B. E. *et al.* A Bivalent Chromatin Structure Marks Key Developmental Genes in Embryonic Stem Cells. *Cell* **125**, 315–326 (2006).
5. van Mierlo, G. *et al.* Integrative Proteomic Profiling Reveals PRC2-Dependent Epigenetic Crosstalk Maintains Ground-State Pluripotency. *Cell Stem Cell* **24**, 123–137.e8 (2019).
6. Chen, K. *et al.* Neurodegenerative Disease Proteinopathies Are Connected to Distinct Histone Post-translational Modification Landscapes. *ACS Chem. Neurosci.* **9**, 838–848 (2018).
7. Kontopoulos, E., Parvin, J. D. & Feany, M. B. Alpha-synuclein acts in the nucleus to inhibit histone acetylation and promote neurotoxicity. *Hum. Mol. Genet.* **15**, 3012–3023 (2006).
8. Fraga, M. F. *et al.* Loss of acetylation at Lys16 and trimethylation at Lys20 of histone H4 is a common hallmark of human cancer. *Nat. Genet.* **37**, 391–400 (2005).
9. van der Kroef, M. *et al.* Histone modifications underlie monocyte dysregulation in patients with systemic sclerosis, underlining the treatment potential of epigenetic targeting. *Ann. Rheum. Dis.* **78**, 529–538 (2019).
10. Govaert, E. *et al.* Extracting histones for the specific purpose of label-free MS. *Proteomics* **16**, 2937–2944 (2016).
11. Noberini, R., Robusti, G. & Bonaldi, T. Mass spectrometry-based characterization of histones in clinical samples: applications, progress, and challenges. *FEBS J.* **289**, 1191–1213 (2022).
12. Sidoli, S., Bhanu, N. V., Karch, K. R., Wang, X. & Garcia, B. A. Complete Workflow for Analysis of Histone Post-translational Modifications Using Bottom-up Mass Spectrometry: From Histone Extraction to Data Analysis. *J. Vis. Exp.* (2016) doi:10.3791/54112.
13. Buenrostro, J. D. *et al.* Single-cell chromatin accessibility reveals principles of regulatory variation. *Nature* **523**, 486–490 (2015).
14. Kieffer, Y. *et al.* Single-Cell Analysis Reveals Fibroblast Clusters Linked to Immunotherapy Resistance in Cancer. *Cancer Discov.* **10**, 1330–1351 (2020).
15. Lawson, D. A. *et al.* Single-cell analysis reveals a stem-cell program in human metastatic breast cancer cells. *Nature* **526**, 131–135 (2015).
16. Gou, B. *et al.* Single-Cell Analysis Reveals Transcriptomic Reprogramming in Aging Cardiovascular Endothelial Cells. *Front Cardiovasc Med* **9**, 900978 (2022).
17. Cheung, P. *et al.* Single-Cell Chromatin Modification Profiling Reveals Increased Epigenetic Variations with Aging. *Cell* **173**, 1385–1397.e14 (2018).
18. Aissa, A. F. *et al.* Single-cell transcriptional changes associated with drug tolerance and response to combination therapies in cancer. *Nat. Commun.* **12**, 1628 (2021).
19. Kreso, A. & Dick, J. E. Evolution of the cancer stem cell model. *Cell Stem Cell* **14**, 275–291 (2014).
20. Rotem, A. *et al.* Single-cell ChIP-seq reveals cell subpopulations defined by chromatin state. *Nat. Biotechnol.* **33**, 1165–1172 (2015).
21. Ku, W. L. *et al.* Single-cell chromatin immunocleavage sequencing (scChIC-seq) to profile histone modification. *Nat. Methods* **16**, 323–325 (2019).
22. Kaya-Okur, H. S. *et al.* CUT&Tag for efficient epigenomic profiling of small samples and single cells. *Nat. Commun.* **10**, 1–10 (2019).
23. Fuchs, S. M., Krajewski, K., Baker, R. W., Miller, V. L. & Strahl, B. D. Influence of combinatorial histone modifications on antibody and effector protein recognition. *Curr. Biol.* **21**, 53–58 (2011).

24. Egelhofer, T. A. *et al.* An assessment of histone-modification antibody quality. *Nat. Struct. Mol. Biol.* **18**, 91–93 (2011).
25. Lu, C., Coradin, M., Porter, E. G. & Garcia, B. A. Accelerating the Field of Epigenetic Histone Modification Through Mass Spectrometry-Based Approaches. *Mol. Cell. Proteomics* **20**, 100006 (2021).
26. Verhelst, S. *et al.* Comprehensive histone epigenetics: A mass spectrometry based screening assay to measure epigenetic toxicity. *MethodsX* **7**, 101055 (2020).
27. Schoof, E. M. *et al.* Quantitative single-cell proteomics as a tool to characterize cellular hierarchies. *Nat. Commun.* **12**, 3341 (2021).
28. Petelski, A. A. *et al.* Multiplexed single-cell proteomics using SCoPE2. *Nat. Protoc.* **16**, 5398–5425 (2021).
29. Rodriguez-Collazo, P., Leuba, S. H. & Zlatanova, J. Robust methods for purification of histones from cultured mammalian cells with the preservation of their native modifications. *Nucleic Acids Res.* **37**, e81 (2009).
30. Dele-Oni, D. O. *et al.* Proteomic profiling dataset of chemical perturbations in multiple biological backgrounds. *Sci Data* **8**, 226 (2021).
31. Matzinger, M., Müller, E., Dürnberger, G., Pichler, P. & Mechtler, K. Robust and Easy-to-Use One-Pot Workflow for Label-Free Single-Cell Proteomics. *Anal. Chem.* **95**, 4435–4445 (2023).
32. Ctortecka, C. *et al.* An Automated Nanowell-Array Workflow for Quantitative Multiplexed Single-Cell Proteomics Sample Preparation at High Sensitivity. *Mol. Cell. Proteomics* **22**, 100665 (2023).
33. Tsai, C.-F. *et al.* Surfactant-assisted one-pot sample preparation for label-free single-cell proteomics. *Commun Biol* **4**, 265 (2021).
34. Yuan, Z.-F. *et al.* EpiProfile 2.0: A Computational Platform for Processing Epi-Proteomics Mass Spectrometry Data. *J. Proteome Res.* **17**, 2533–2541 (2018).
35. Wiśniewski, J. R., Hein, M. Y., Cox, J. & Mann, M. A 'proteomic ruler' for protein copy number and concentration estimation without spike-in standards. *Mol. Cell. Proteomics* **13**, 3497–3506 (2014).
36. Sidoli, S. *et al.* One minute analysis of 200 histone posttranslational modifications by direct injection mass spectrometry. *Genome Res.* **29**, 978–987 (2019).
37. Guo, Q., Sidoli, S., Garcia, B. A. & Zhao, X. Assessment of Quantification Precision of Histone Post-Translational Modifications by Using an Ion Trap and down To 50 000 Cells as Starting Material. *J. Proteome Res.* **17**, 234–242 (2018).
38. Sidoli, S., Lin, S., Karch, K. R. & Garcia, B. A. Bottom-up and middle-down proteomics have comparable accuracies in defining histone post-translational modification relative abundance and stoichiometry. *Anal. Chem.* **87**, 3129–3133 (2015).
39. Sidoli, S., Simithy, J., Karch, K. R., Kulej, K. & Garcia, B. A. Low Resolution Data-Independent Acquisition in an LTQ-Orbitrap Allows for Simplified and Fully Untargeted Analysis of Histone Modifications. *Anal. Chem.* **87**, 11448–11454 (2015).
40. Keenan, A. B. *et al.* The Library of Integrated Network-Based Cellular Signatures NIH Program: System-Level Cataloging of Human Cells Response to Perturbations. *Cell Syst* **6**, 13–24 (2018).
41. Stransky, S., Cutler, R., Aguilan, J., Nieves, E. & Sidoli, S. Investigation of reversible histone acetylation and dynamics in gene expression regulation using 3D liver spheroid model. *Epigenetics Chromatin* **15**, 35 (2022).
42. Lee, J.-S., Smith, E. & Shilatifard, A. The language of histone crosstalk. *Cell* **142**, 682–685 (2010).
43. Price, A. J., Manjegowda, M. C., Kain, J., Anandh, S. & Bochkis, I. M. Hdac3, Setdb1, and Kap1 mark H3K9me3/H3K14ac bivalent regions in young and aged liver. *Aging Cell* **19**, e13092 (2020).

44. Sidoli, S. *et al.* A mass spectrometry-based assay using metabolic labeling to rapidly monitor chromatin accessibility of modified histone proteins. *Sci. Rep.* **9**, 13613 (2019).
45. Hayashi, T., Daitoku, H., Uetake, T., Kako, K. & Fukamizu, A. Histidine Nτ-methylation identified as a new posttranslational modification in histone H2A at His-82 and H3 at His-39. *J. Biol. Chem.* **299**, 105131 (2023).
46. Orsburn, B. C. Metabolomic, Proteomic, and Single-Cell Proteomic Analysis of Cancer Cells Treated with the KRASG12D Inhibitor MRTX1133. *J. Proteome Res.* **22**, 3703–3713 (2023).
47. Orsburn, B. C. Single cell proteomics by mass spectrometry reveals deep epigenetic insight and new targets of a class specific histone deacetylase inhibitor. *bioRxiv* (2024) doi:10.1101/2024.01.05.574437.
48. Derks, J. *et al.* Increasing the throughput of sensitive proteomics by plexDIA. *Nat. Biotechnol.* **41**, 50–59 (2023).
49. Searfoss, R. M., Karki, R., Lin, Z., Robison, F. & Garcia, B. A. An Optimized and High-Throughput Method for Histone Propionylation and Data-Independent Acquisition Analysis for the Identification and Quantification of Histone Post-translational Modifications. *J. Am. Soc. Mass Spectrom.* **34**, 2508–2517 (2023).
50. Ritchie, M. E. *et al.* limma powers differential expression analyses for RNA-sequencing and microarray studies. *Nucleic Acids Res.* **43**, e47 (2015).
51. Blighe, K. *PCAtools: PCAtools: Everything Principal Components Analysis*. (Github).
52. Gu, Z. Complex heatmap visualization. *Imeta* **1**, e43 (2022).
53. Taiyun. *Corrplot: A Visual Exploratory Tool on Correlation Matrix*. (Github).

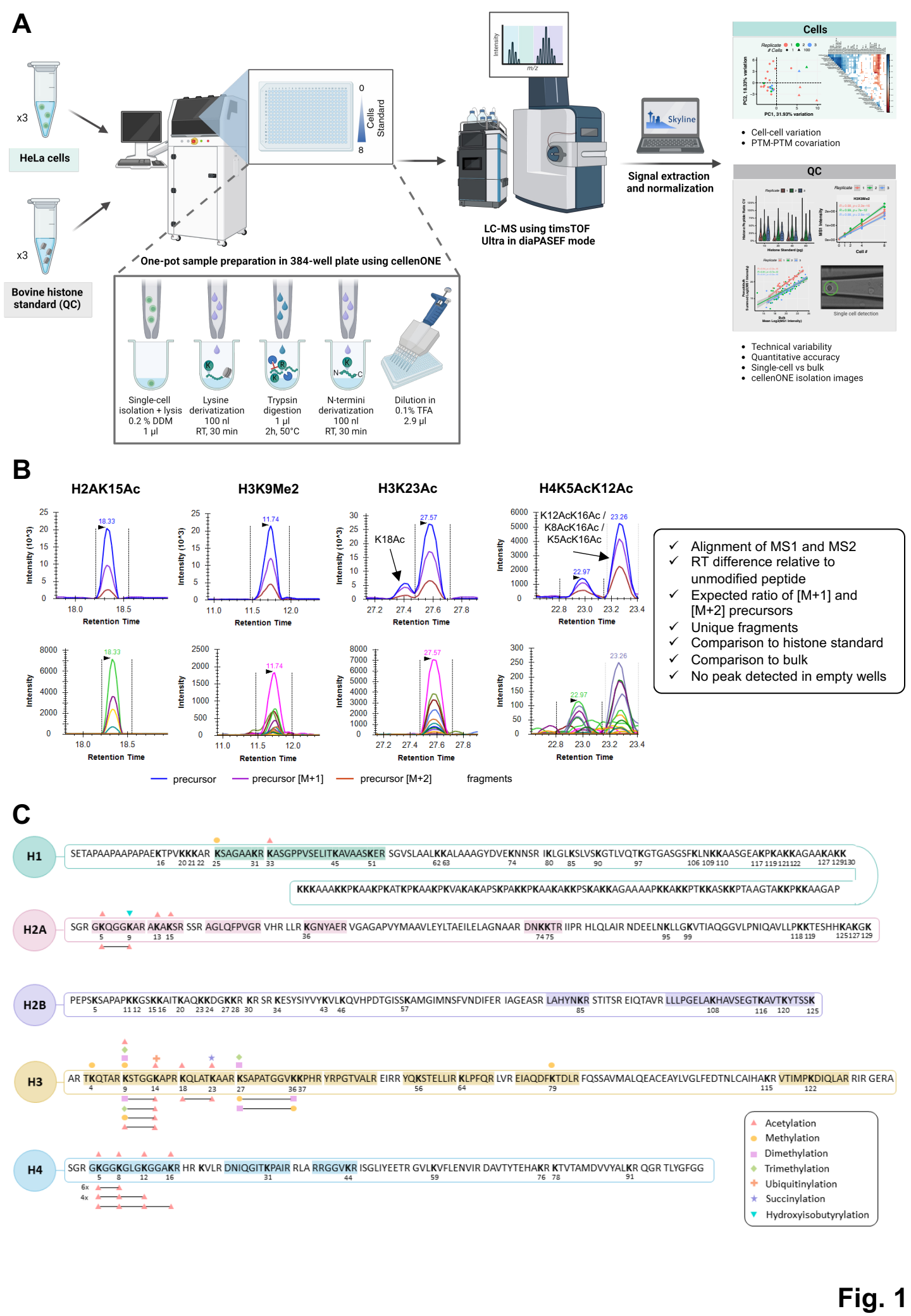
A
x3
HeLa cells
x3
Bovine histone standard (QC)
0
Cells
Standard
8
One-pot sample preparation in 384-well plate using cellenONE
Single-cell isolation + lysis 0.2 % DDM 1 µl
Lysine derivatization 100 nl RT, 30 min
Trypsin digestion 1 µl 2h, 50°C
N-termini derivatization 100 nl RT, 30 min
Dilution in 0.1% TFA 2.9 µl
Intensity
m/z
LC-MS using timsTOF Ultra in diaPASEF mode
Skyline
Signal extraction and normalization
Cells
Cell-cell variation
PTM-PTM covariation
QC
Single cell detection
Technical variability
Quantitative accuracy
Single-cell vs bulk
cellenONE isolation images
B
H2AK15Ac
H3K9Me2
H3K23Ac
H4K5AcK12Ac
Intensity (10^3)
Intensity
Retention Time
18.33
11.74
27.57
23.26
22.97
K18Ac
K12AcK16Ac / K8AcK16Ac / K5AcK16Ac
precursor
precursor [M+1]
precursor [M+2]
fragments
✓ Alignment of MS1 and MS2
✓ RT difference relative to unmodified peptide
✓ Expected ratio of [M+1] and [M+2] precursors
✓ Unique fragments
✓ Comparison to histone standard
✓ Comparison to bulk
✓ No peak detected in empty wells
C
H1
SETAPAAPAAPAPAEKTPVKKKAR KSAGAAKR KASGPPVSELITKAVAASKER SGVSLAALKKALAAAGYDVEKNNSR IKLGLKSLVSKGTLVQTKGTGASGSFKLNKKAASGEAKPKAKKAGAAKAKK
KKKAAAKKPKAAKPKATKPKAAKPKVAKAKAPSKPAKKPKAAKAKKPSKAKKAGAAAAPKKAKKPTKKASKKPTAAGTAKKPKKAAGAP
H2A
SGR GKQGGKAR AKAKSR SSR AGLQFPVGR VHR LLR KGNYAER VGAGAPVYMAAVLEYLTAEILELAGNAAR DNKKTR IIPR HLQLAIR NDEELNKLLGKVTIAQGGVLPNIQAVLLPKKTESHHKAKGK
H2B
PEPSKSAPAPKKGSKKAITKAQKKDGKKR KR SR KESYSIYVYKVLKQVHPDTGISSKAMGIMNSFVNDIFER IAGEASR LAHYNKR STITSR EIQTAVR LLLPGELAKHAVSEGTKAVTKYTSSK
H3
AR TKQTAR KSTGGKAPR KQLATKAAR KSAPATGGVKKPHR YRPGTVALR EIRR YQKSTELLIR KLPFQR LVR EIAQDFKTDLR FQSSAVMALQEACEAYLVGLFEDTNLCAIHAKR VTIMPKDIQLAR RIR GERA
H4
SGR GKGGKGLGKGGAKR HR KVLR DNIQGITKPAIR RLA RRGGVKR ISGLIYEETR GVLKVFLENVIR DAVTYTEHAKR KTVTAMDVVYALKR QGR TLYGFGG
6x
4x
Acetylation
Methylation
Dimethylation
Trimethylation
Ubiquitinylation
Succinylation
Hydroxyisobutyrylation

Fig. 1

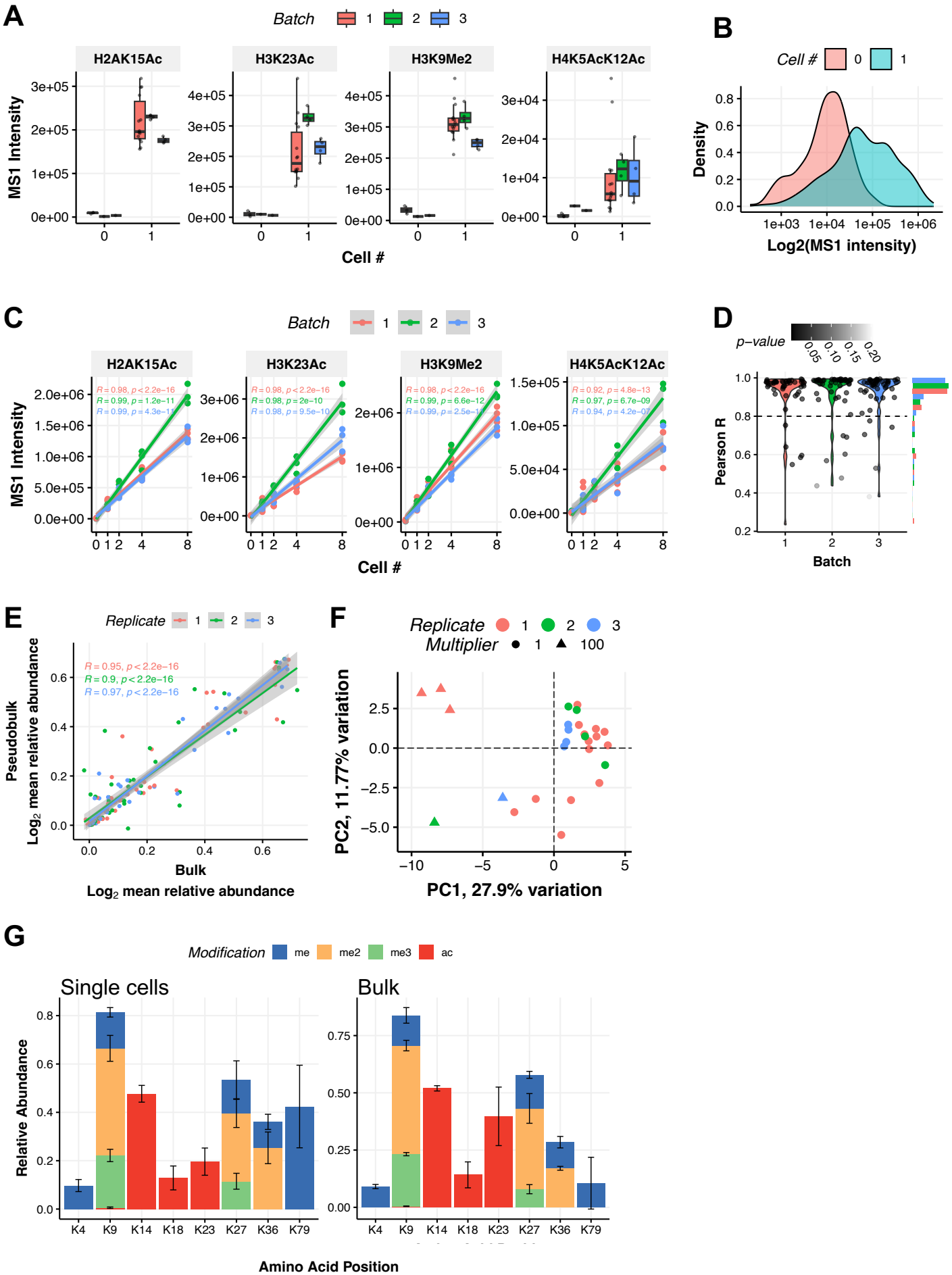
A
Batch 1 2 3
H2AK15Ac
H3K23Ac
H3K9Me2
H4K5AcK12Ac
MS1 Intensity
Cell #
B
Cell # 0 1
Density
Log2(MS1 intensity)
C
Batch 1 2 3
H2AK15Ac
H3K23Ac
H3K9Me2
H4K5AcK12Ac
MS1 Intensity
Cell #
D
p−value
Pearson R
Batch
E
Replicate 1 2 3
R = 0.95, p < 2.2e−16
R = 0.9, p < 2.2e−16
R = 0.97, p < 2.2e−16
Pseudobulk
Log2 mean relative abundance
Bulk
Log2 mean relative abundance
F
Replicate 1 2 3
Multiplier 1 100
PC2, 11.77% variation
PC1, 27.9% variation
G
Modification me me2 me3 ac
Single cells
Bulk
Relative Abundance
K4 K9 K14 K18 K23 K27 K36 K79
Amino Acid Position

Fig. 2

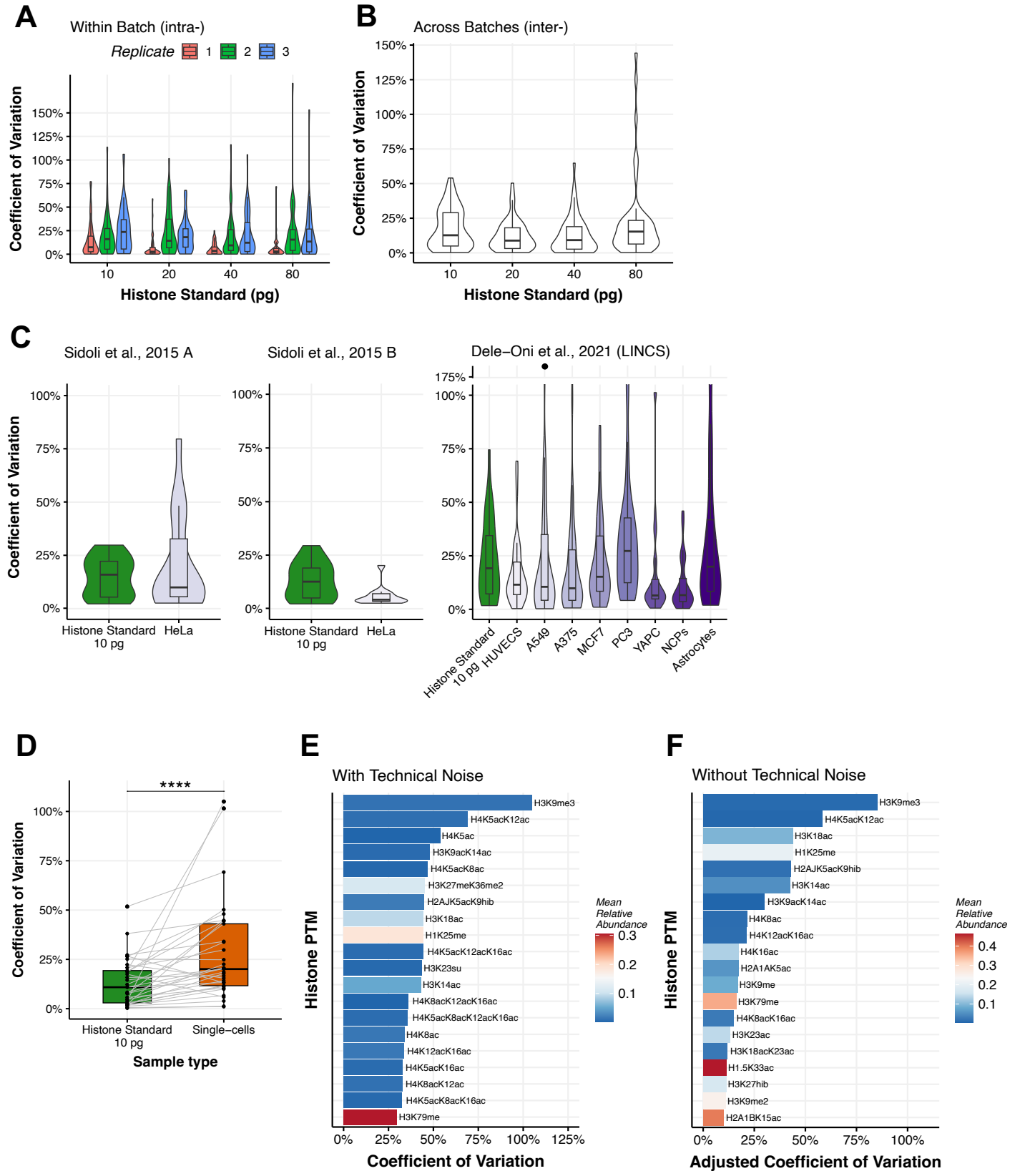
A
Within Batch (intra-)
Replicate 1 2 3
Coefficient of Variation
150%
125%
100%
75%
50%
25%
0%
10
20
40
80
Histone Standard (pg)
B
Across Batches (inter-)
Coefficient of Variation
150%
125%
100%
75%
50%
25%
0%
10
20
40
80
Histone Standard (pg)
C
Sidoli et al., 2015 A
Sidoli et al., 2015 B
Dele–Oni et al., 2021 (LINCS)
Coefficient of Variation
100%
75%
50%
25%
0%
175%
Histone Standard 10 pg
HeLa
HUVECS
A549
A375
MCF7
PC3
YAPC
NCPs
Astrocytes
D
****
Coefficient of Variation
100%
75%
50%
25%
0%
Histone Standard 10 pg
Single–cells
Sample type
E
With Technical Noise
Histone PTM
H3K9me3
H4K5acK12ac
H4K5ac
H3K9acK14ac
H4K5acK8ac
H3K27meK36me2
H2AJK5acK9hib
H3K18ac
H1K25me
H4K5acK12acK16ac
H3K23su
H3K14ac
H4K8acK12acK16ac
H4K5acK8acK12acK16ac
H4K8ac
H4K12acK16ac
H4K5acK16ac
H4K8acK12ac
H4K5acK8acK16ac
H3K79me
Mean Relative Abundance
0.3
0.2
0.1
0%
25%
50%
75%
100%
125%
Coefficient of Variation
F
Without Technical Noise
Histone PTM
H3K9me3
H4K5acK12ac
H3K18ac
H1K25me
H2AJK5acK9hib
H3K14ac
H3K9acK14ac
H4K8ac
H4K12acK16ac
H4K16ac
H2A1AK5ac
H3K9me
H3K79me
H4K8acK16ac
H3K23ac
H3K18acK23ac
H1.5K33ac
H3K27hib
H3K9me2
H2A1BK15ac
Mean Relative Abundance
0.4
0.3
0.2
0.1
0%
25%
50%
75%
100%
Adjusted Coefficient of Variation

Fig. 3

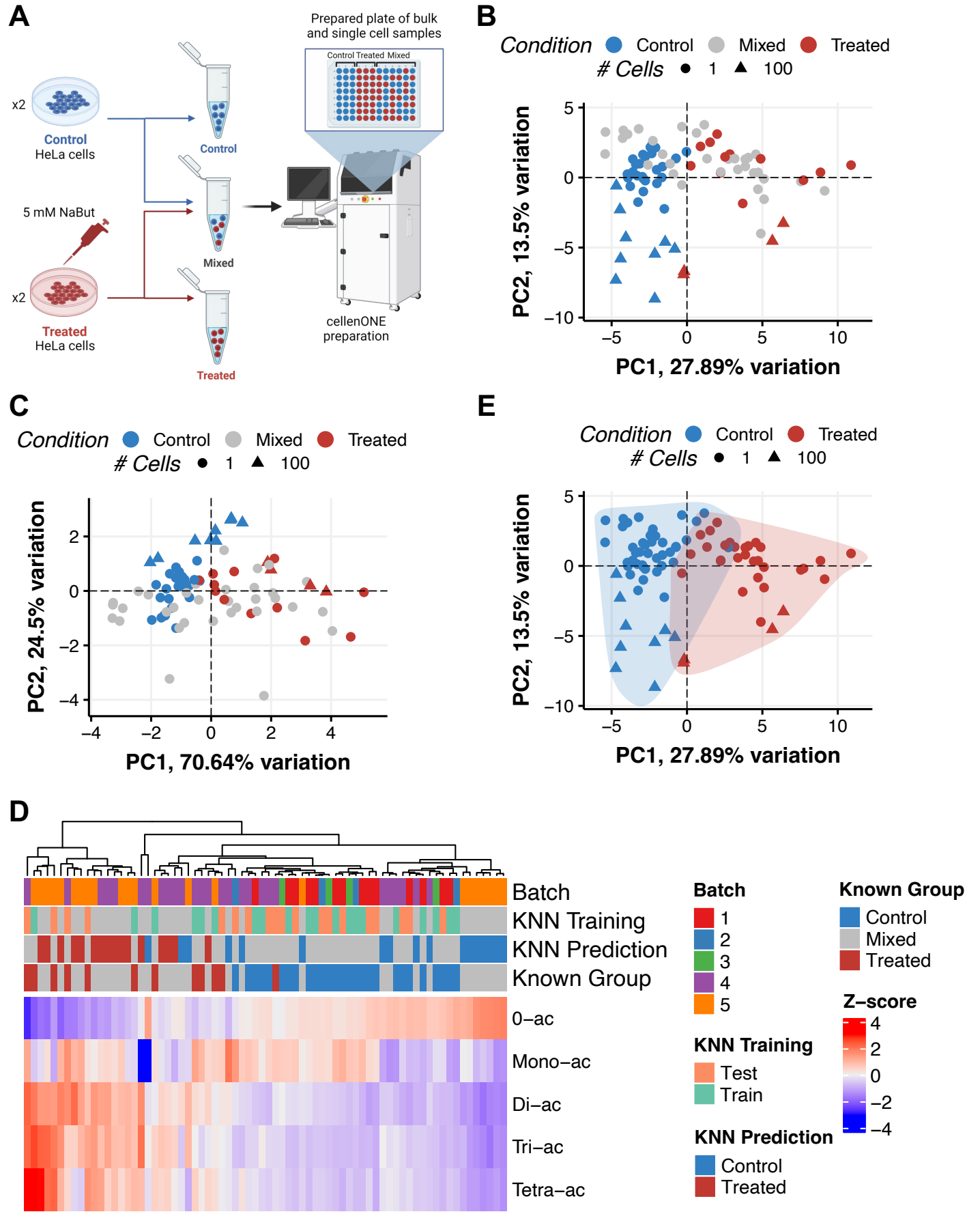
A
Prepared plate of bulk and single cell samples
Control Treated Mixed
x2
Control
HeLa cells
Control
5 mM NaBut
Mixed
x2
Treated
HeLa cells
Treated
cellenONE preparation
B
Condition Control Mixed Treated
Cells 1 100
PC2, 13.5% variation
PC1, 27.89% variation
C
Condition Control Mixed Treated
Cells 1 100
PC2, 24.5% variation
PC1, 70.64% variation
E
Condition Control Treated
Cells 1 100
PC2, 13.5% variation
PC1, 27.89% variation
D
Batch
KNN Training
KNN Prediction
Known Group
0–ac
Mono–ac
Di–ac
Tri–ac
Tetra–ac
Batch
1
2
3
4
5
KNN Training
Test
Train
KNN Prediction
Control
Treated
Known Group
Control
Mixed
Treated
Z–score
4
2
0
–2
–4

Fig. 4

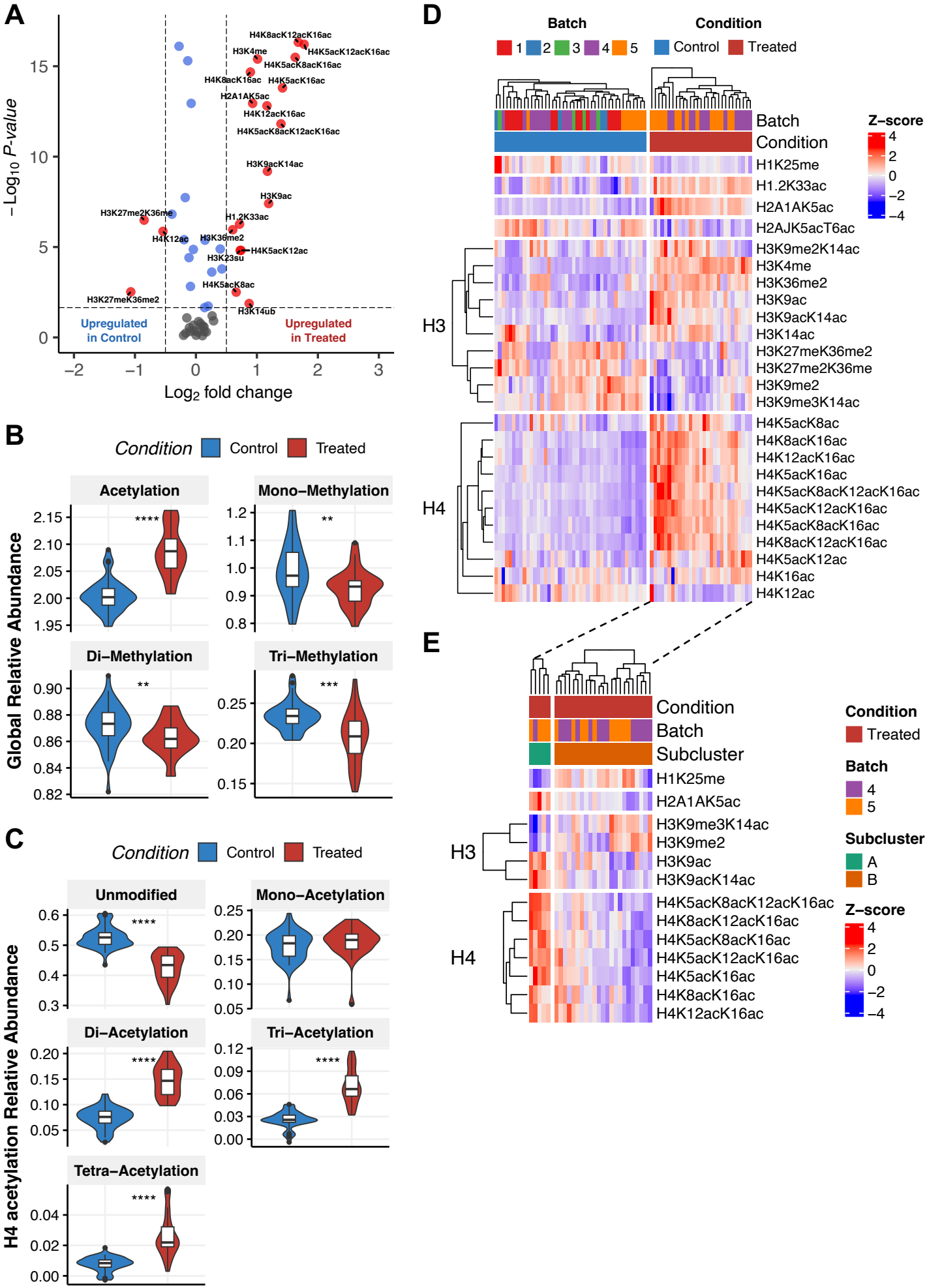
A
−Log10 P-value
Log2 fold change
H4K8acK12acK16ac
H4K5acK12acK16ac
H3K4me
H4K5acK8acK16ac
H4K8acK16ac
H4K5acK16ac
H2A1AK5ac
H4K12acK16ac
H4K5acK8acK12acK16ac
H3K9acK14ac
H3K9ac
H3K27me2K36me
H1.2K33ac
H4K12ac
H3K36me2
H4K5acK12ac
H3K23su
H4K5acK8ac
H3K27meK36me2
H3K14ub
Upregulated in Control
Upregulated in Treated
B
Condition
Control
Treated
Acetylation
Mono−Methylation
Di−Methylation
Tri−Methylation
Global Relative Abundance
C
Condition
Control
Treated
Unmodified
Mono−Acetylation
Di−Acetylation
Tri−Acetylation
Tetra−Acetylation
H4 acetylation Relative Abundance
D
Batch
Condition
Control
Treated
Z−score
H1K25me
H1.2K33ac
H2A1AK5ac
H2AJK5acT6ac
H3K9me2K14ac
H3K4me
H3K36me2
H3K9ac
H3K9acK14ac
H3K14ac
H3K27meK36me2
H3K27me2K36me
H3K9me2
H3K9me3K14ac
H3
H4K5acK8ac
H4K8acK16ac
H4K12acK16ac
H4K5acK16ac
H4K5acK8acK12acK16ac
H4K5acK12acK16ac
H4K5acK8acK16ac
H4K8acK12acK16ac
H4K5acK12ac
H4K16ac
H4K12ac
H4
E
Condition
Batch
Subcluster
H1K25me
H2A1AK5ac
H3K9me3K14ac
H3K9me2
H3K9ac
H3K9acK14ac
H3
H4K5acK8acK12acK16ac
H4K8acK12acK16ac
H4K5acK8acK16ac
H4K5acK12acK16ac
H4K5acK16ac
H4K8acK16ac
H4K12acK16ac
H4

Fig. 5

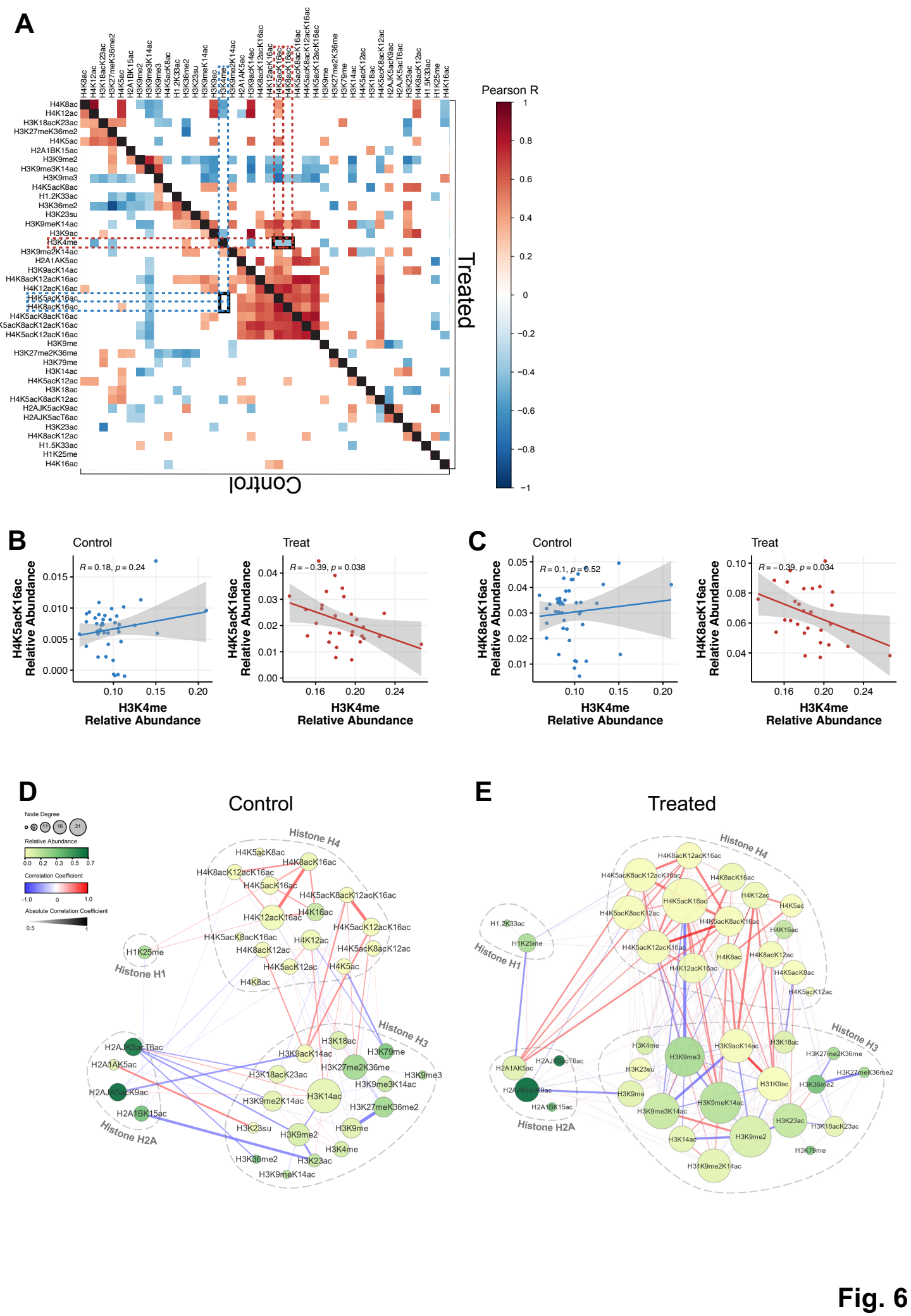
A
Pearson R
Treated
Control
B
Control
Treat
H4K5acK16ac Relative Abundance
H3K4me Relative Abundance
R = 0.18, p = 0.24
R = −0.39, p = 0.038
C
Control
Treat
H4K8acK16ac Relative Abundance
H3K4me Relative Abundance
R = 0.1, p = 0.52
R = −0.39, p = 0.034
D
Control
Node Degree
Relative Abundance
Correlation Coefficient
Absolute Correlation Coefficient
Histone H4
Histone H1
Histone H3
Histone H2A
E
Treated
Histone H4
Histone H1
Histone H3
Histone H2A

Fig. 6